resistance to physiologic oxidative stress. *Cell.* 2007;128(2):325-339.

21. Miyamoto K, Araki KY, Naka K, et al. Foxo3a is essential for maintenance of the hematopoietic stem cell pool. *Cell Stem Cell.* 2007;1(1):101-112.
22. Tsai WB, Chung YM, Takahashi Y, Xu Z, Hu MC. Functional interaction between FOXO3a and ATM regulates DNA damage response. *Nat Cell Biol.* 2008;10(4):460-467.
23. Bakkenist CJ, Kastan MB. DNA damage activates ATM through intermolecular autophosphorylation and dimer dissociation. *Nature.* 2003;421(6922):499-506.
24. Wilson A, Laurenti E, Oser G, et al. Hematopoietic stem cells reversibly switch from dormancy to self-renewal during homeostasis and repair. *Cell.* 2008;135(6):1118-1129.
25. Foudi A, Hochedlinger K, Van Buren D, et al. Analysis of histone 2B-GFP retention reveals slowly cycling hematopoietic stem cells. *Nat Biotechnol.* 2009;27(1):84-90.
26. Mohrin M, Bourke E, Alexander D, et al. Hematopoietic stem cell quiescence promotes error-prone DNA repair and mutagenesis. *Cell Stem Cell.* 2010;7(2):174-185.
27. Milyavsky M, Gan OI, Trottier M, et al. A distinctive DNA damage response in human hematopoietic stem cells reveals an apoptosis-independent role for p53 in self-renewal. *Cell Stem Cell.* 2010;7(2):186-197.
28. Gazit R, Weissman IL, Rossi DJ. Hematopoietic stem cells and the aging hematopoietic system. *Semin Hematol.* 2008;45(4):218-224.
29. Bondar T, Medzhitov R. p53-mediated hematopoietic stem and progenitor cell competition. *Cell Stem Cell.* 2010;6(4):309-322.
30. Marusyk A, Porter CC, Zaberezhnyy V, DeGregori J. Irradiation selects for p53-deficient hematopoietic progenitors. *PLoS Biol.* 2010;8(3):e1000324.

A novel animal model of Epstein-Barr virus–associated hemophagocytic lymphohistiocytosis in humanized mice

Kei Sato,[1,2] Naoko Misawa,[1] Chuanyi Nie,[1] Yorifumi Satou,[3] Dai Iwakiri,[4] Masao Matsuoka,[3] Rei Takahashi,[5,6] Kiyotaka Kuzushima,[7] Mamoru Ito,[8] Kenzo Takada,[4] and Yoshio Koyanagi[1]

[1]Laboratory of Virus Pathogenesis, [2]Center for Emerging Virus Research, and [3]Laboratory of Viral Control, Institute for Virus Research, Kyoto University, Kyoto, Japan; [4]Department of Tumor Virology, Institute for Genetic Medicine, Hokkaido University, Sapporo, Japan; [5]Pathology and Tumor Biology, Graduate School of Medicine, Kyoto University, Kyoto, Japan; [6]Doshisha Women's College of Liberal Arts, Kyotanabe, Japan; [7]Laboratory of Viral Oncology, Aichi Cancer Center, Nagoya, Japan; and [8]Central Institute for Experimental Animals, Kawasaki, Japan

EBV-associated hemophagocytic lymphohistiocytosis (EBV-HLH) is a rare yet devastating disorder caused by EBV infection in humans. However, the mechanism of this disease has yet to be elucidated because of a lack of appropriate animal models. Here, we used a human CD34$^+$ cell-transplanted humanized mouse model and reproduced pathologic conditions resembling EBV-HLH in humans. By 10 weeks postinfection, two-thirds of the infected mice died after exhibiting high and persistent viremia, leukocytosis, IFN-γ cytokinenemia, normocytic anemia, and thrombocytopenia. EBV-infected mice also showed systemic organ infiltration by activated CD8$^+$ T cells and prominent hemophagocytosis in BM, spleen, and liver. Notably, the level of EBV load in plasma correlated directly with both the activation frequency of CD8$^+$ T cells and the level of IFN-γ in plasma. Moreover, high levels of EBV-encoded small RNA1 were detected in plasma of infected mice, reflecting what has been observed in patients. These findings suggest that our EBV infection model mirrors virologic, hematologic, and immunopathologic aspects of EBV-HLH. Furthermore, in contrast to CD8$^+$ T cells, we found a significant decrease of natural killer cells, myeloid dendritic cells, and plasmacytoid dendritic cells in the spleens of infected mice, suggesting that the collapse of balanced immunity associates with the progression of EBV-HLH pathogenesis. (Blood. 2011;117(21):5663-5673)

Introduction

EBV is a human-specific double-stranded DNA virus that belongs to Gammaherpesvirinae.[1] EBV is one of the most commonly found viruses in humans, infecting 90% of adults worldwide.[1] Primary infection of EBV can manifest into infectious mononucleosis, which is a condition characterized by lymphadenopathy and the appearance of atypical CD8$^+$ T cells in the peripheral blood (PB).[1,2] Infectious mononucleosis is usually a self-limiting and nonlife-threatening condition that does not require specific treatment.[1,2] However, EBV infection can also result in serious conditions such as Burkitt lymphoma, Hodgkin lymphoma, and other B-cell lymphomas.[1,2] Among the disorders induced by EBV infection, hemophagocytic lymphohistiocytosis (HLH) is one of the most devastating.

HLH is an immunopathologic entity characterized by an uncontrolled activation of the immune system.[3-5] In patients with HLH, persistent activation of CD8$^+$ T cells and innate immune cells lead to the overproduction of proinflammatory cytokines such as IFN-γ and TNF-α.[3] The elevated concentration of the proinflammatory cytokines drives further proliferation and activation of CD8$^+$ T cells and macrophages/histiocytes.[3] Activated macrophages/histiocytes engulf blood cells, a process called hemophagocytosis, and cause erythrocytopenia and thrombocytopenia.[3-5] Activated CD8$^+$ T cells invade organs systemically, causing hepatomegaly, splenomegaly, inflammation, and organ failure.[3-6]

The mortality rate of HLH can be as high as 50% even with treatment.[6] Currently, there are no specific therapies against HLH[3,6] and options for HLH therapy are limited to supportive care and combined immunosuppressive regimens. However, the latter treatment can lead to complications such as life-threatening infections.

HLH can be categorized into 2 types, congenital HLH and acquired HLH. Congenital HLH is associated with predisposing genetic mutations, whereas acquired HLH is not. In one example of congenital HLH, mutations in PRF1 (encodes Perforin) cause impaired cytolytic granule formation, which leads to the development of HLH.[7,8] X-linked lymphoproliferative syndrome (XLP) is also one of the congenital HLHs and is followed by primary EBV infection. Genetic mutations in SAP/SH2D1A (encodes SLAM-associated protein [SAP])[9] or XIAP/BIRC4 (encodes X-linked inhibitor-of-apoptosis [XIAP])[10] are responsible for XLP. Dysfunction of SAP can cause multiple immune impairments, including inefficient effector function of HLA-restricted EBV-specific CTLs,[11] whereas dysfunction of XIAP leads to the deregulation of lymphocyte homeostasis.[10]

To reproduce the pathogenesis of congenital HLH, representative mouse models have been reported.[12,13] For instance, Sap (encodes Sap, the ortholog of SAP/SH2D1A in human) knockout mice,[13] and Prf (encodes Perforin) knockout mice[12] exhibit XLP-like disorders after infection with lymphocytic choriomeningitis virus (LCMV). These LCMV-infected knockout mice showed

Submitted September 10, 2010; accepted March 16, 2011. Prepublished as *Blood* First Edition paper, April 5, 2011; DOI 10.1182/blood-2010-09-305979.

The online version of this article contains a data supplement.

The publication costs of this article were defrayed in part by page charge payment. Therefore, and solely to indicate this fact, this article is hereby marked "advertisement" in accordance with 18 USC section 1734.

persistent activation of $CD8^+$ T cells, elevated proinflammatory cytokines, including IFN-γ and TNF-α in plasma, and high rates of mortality.[12,13] LCMV-infected Prf knockout mice also displayed hepatosplenomegaly, anemia, and activation of phagocytes.[12]

In contrast to congenital HLH, acquired HLH is not associated with any genetic defects but can be triggered by malignancies and/or infections.[3-5] As an animal model of acquired HLH, it has been recently reported that a conventional mouse infected with Salmonella enterica serotype typhimurium exhibits HLH-like disorders.[14] However, bacterial infection-associated HLH only represents a small fraction of infection-associated HLH in humans.[7] EBV is responsible for up to 70% of infection-associated HLH in humans.[15] Therefore, it is important to reproduce the pathogenesis of EBV-HLH in experimental models with human immunity.

To reproduce human immunity and the diseases caused by human-specific pathogens such as HIV-1 and EBV in animals, humanized mouse models have been generated by transplanting human $CD34^+$ hematopoietic stem cells (hHSCs) into lines of immunodeficient mice.[16-21] Previous studies on EBV infection in humanized mouse models were successful in reproducing EBV-associated B-cell malignancies[16,21] and/or human immune responses against EBV antigens.[17,18,20,21] However, none so far has shown EBV-HLH in humanized mice.

In this study, we demonstrate a humanized mouse model of EBV-HLH. The infection of newborn immunodeficient mice xenotransplanted with hHSCs (NOG-hCD34 mice) with EBV resulted in cardinal features of HLH, including hemophagocytosis, erythrocytopenia, thrombocytopenia, hypercytokinemia, $CD8^+$ T-cell activation/proliferation and organ infiltration, and histiocyte proliferation. Moreover, the disease severity, IFN-γ production, and $CD8^+$ T-cell activation correlated with EBV DNA production.

Methods

Generation of NOG-hCD34 mice

NOD/ShiJic-scid $\gamma_c^{-/-}$ (NOG) mice[22] were obtained from the Central Institute for Experimental Animals. The mice were maintained under specific pathogen-free conditions and were handled in accordance with the Regulation on Animal Experimentation at Kyoto University. Fresh human cord blood was obtained with the parent's written informed consent from healthy full-term newborns, and $CD34^+$ hHSCs were purified and transplanted into NOG mice as previously described.[23-25] HLA class I typing was performed by an HLA laboratory, and the results are summarized in supplemental Table 1 (available on the Blood Web site; see the Supplemental Materials link at the top of the online article). Body weights of mice were routinely measured, and the mice were anesthetized and killed when the weights became < 75% of their maximum weight or at 10 weeks postinfection (wpi).

Virus preparation and infection

EBV (strain Akata) was prepared and titrated as described previously.[26] One thousand TD_{50} of EBV solution or RPMI (for mock-infection) was intravenously inoculated into NOG-hCD34 mice between 13 and 16 weeks of age.

PB collection and isolation of nucleated cells from organs

PB was collected weekly as described previously.[23-25] Mononuclear cells (MNCs) in PB (PBMCs), spleen, BM, liver, lung, kidney, and ascitic lavage fluid were collected as previously described.[23-25] Human leukocytes were further purified from the MNCs by the use of Ficoll-Paque (Pharmacia), and murine leukocytes were purified from the MNCs by the use of lympholyte-M (Cedarlane Ltd).

Hemocytometry

The levels of leukocytes, erythrocytes, platelets, hematocrit, and hemoglobin in PB and the levels of mean cell volume (MCV), mean cell hemoglobin (MCH), and mean cell hemoglobin concentration (MCHC) in erythrocytes were measured by Celltac α MEK-6450 (Nihon Kohden Co).

Flow cytometry and cell sorting

Flow cytometry was performed with FACSCalibur and FACSCanto (BD Biosciences) as previously described.[23-25,27,28] Anti–human CD45RA-biotin, CD45RO-APC, HLA-DR-PE, Ki67-PE (BD Biosciences), CD11c-APC, CD56-FITC, FOXP3-PE (BioLegend), CD3-PE, CD4-PE, CD8-FITC, CD8-APC, CD19-FITC (Dakocytomation), CD45-biotin (eBiosciences), CD38-biotin, CD303-FITC (Miltenyi Biotec), and anti–murine CD45-PE (ImmunoTech) antibodies were used. For detection of biotinylated antibodies, streptavidin-conjugated PerCP (BD Biosciences) was used. Human $CD4^+$, $CD8^+$, $CD19^+$, and murine $CD45^+$ cells were sorted from splenic MNCs by FACSAria (BD Biosciences). The purity of each population was > 95%.

Tetramer staining

PE-conjugated HLA-A*2402 tetramers mounted with 5 different EBV antigen peptides (derived from BRLF1, BMLF1, LMP2, EBNA3A, and EBNA3B) and PE-conjugated HLA-A*2402 tetramers mounted with HIV-1 Gag antigen peptides were purchased from medical and biologic laboratories, and the staining was performed according to manufacturer's protocol.

Histologic analyses

Preparation of frozen organ sections was conducted as previously described.[29] H&E staining, Berlin blue staining, Giemsa staining, and nonspecific esterase (NSE) staining were performed by conventional methods, respectively.

Immunostaining and in situ hybridization

Immunostaining was performed as previously described.[23] Rabbit anti–human CD8 (Lab Vision), mouse anti–human CD68 (BD Biosciences), anti–human CD20 (Dakocytomation), anti-ZEBRA (Santa Cruz Biotechnology), and anti-gp110 (Cl.50-1) monoclonal antibodies were used as primary antibodies, and appropriate secondary antibodies were used for detection. In situ hybridization for EBV-encoded small RNAs (EBERs) was performed by Kyodo Byori Inc.

PCR and RT-PCR

DNA was extracted from whole PB (30 μL), plasma (30 μL), human MNCs, and murine MNCs with the QIAamp DNA Micro kit (QIAGEN) or DNeasy Blood and Tissue kit (QIAGEN). EBV genomic DNA was quantified by real-time PCR as previously described,[30] and EBV quantified viral DNA control (Advanced Biotechnologies) was used as the standard. The cell number was also quantified by real-time PCR with the use of TaqMan β-actin control reagents (Applied Biosystems), and quantified PBMC genomic DNA was used as the standard. RNA was extracted by the use of RNeasy Mini kit (QIAGEN). Primers used for RT-PCR are listed in supplemental Table 2.

Quantification of cytokines and EBV-encoded small RNA1 in plasma

Quantification of IFN-γ and TNF-α in 10 μL of plasma was performed by the use of cytometric bead array system according to the manufacture's protocol (BD Biosciences). Quantification of IFN-β was performed by the use of a human IFN-β ELISA kit (PBL Biomedical Laboratories).

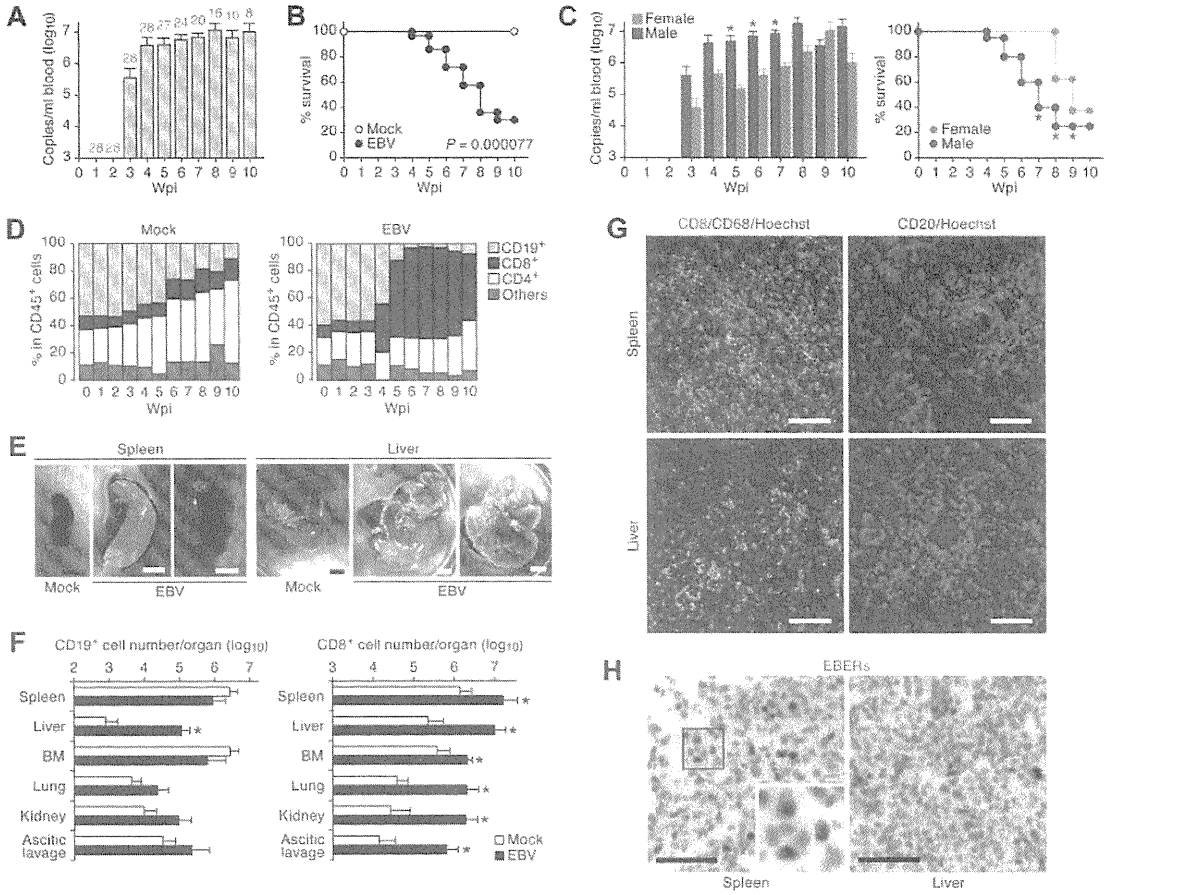

Figure 1. Fatal outcome of EBV-infected NOG-hCD34 mice with persistent viremia, expansion of CD8$^+$ T cells, and hepatosplenomegaly in the absence of B-cell proliferative disorders. (A) Quantification of EBV DNA in the PB of EBV-infected mice. Number at the top of each gray bar represents the number of analyzed EBV-infected mice at each time point. (B) Survival curve. Kaplan-Meier survival curve of mock-infected mice (n = 15) and EBV-infected mice (n = 28) is shown. Statistical significance in the survival rate (P = .000077) between mock-infected mice and EBV-infected mice was determined by log-rank test. (C) The difference in the viremia and the survival rate between male and female recipient mice. (Left) The level of EBV DNA in the PB of EBV-infected male mice (n = 20) and EBV-infected female mice (n = 8). Asterisks represent statistic significance ($P < .05$ by Welch t test) versus the value obtained from EBV-infected female mice. (Right) Survival curve. Kaplan-Meier survival curve of EBV-infected male mice (n = 20) and EBV-infected female mice (n = 8) is shown. Statistical significances in the survival rate between EBV-infected male mice and EBV-infected female mice until the indicated wpi were determined by log-rank test. (D) Longitudinal analysis on human PBMC composition. PB was routinely collected from mock-infected mice (n = 5) and EBV-infected mice (n = 12) and was analyzed by flow cytometry. Results are presented as the average percentages in human CD45$^+$ leukocytes. (E) Hepatosplenomegaly in EBV-infected mice. Representatives of spleens and livers of a mock-infected and 2 EBV-infected mice are shown. Scale bars in panel E represent 5 mm. (F) Human MNC numbers in multiple organs. The cell numbers of CD19$^+$ B cells (left) and CD8$^+$ T cells (right) in spleen, liver, BM, lung, kidney, and ascitic lavage fluid of mock-infected mice (n = 4) and EBV-infected mice (n = 7) are shown. Asterisks represent statistic significance ($P < .05$ by Welch t test) versus the value obtained from the mock-infected mice. (G) Immunostaining for CD8, CD68, and CD20. Representatives of spleen (top) and liver (bottom) of EBV-infected mice, respectively, are shown. CD8$^+$ cells (left) and CD20$^+$ cells (right) are shown in green, CD68$^+$ cells (left) are shown in red, and nuclei were shown in blue by staining with Hoechst. (H) In situ hybridization for EBERs. Representatives of spleen (left) and liver (right) of EBV-infected mice were shown. EBERs were shown in brown. Areas enclosed with squares are enlarged in bottom right of the panel. Scale bars in panels G and H represent 50 μm.

EBV-encoded small RNA1 (EBER1) in plasma was quantified as previously described.[31]

Statistic analyses

Statistic differences were determined by paired t test, Student t test, or Welch t test, and $P < .05$ was considered statistically significant. The log-rank test was adopted to determine the statistical significance of survival rates (Figure 1B-C). To determine the statistically significant correlation, the Spearman rank correlation coefficient (r_s) was adopted (Figure 5E-G). Data are presented as mean ± SEM.

Ethics statement

All protocols involving human subjects were reviewed and approved by the Kyoto University Institutional Review Board. Informed written consents from the human subjects were obtained in this study in accordance with the Declaration of Helsinki.

Results

High mortality from EBV infection with systemic organ infiltration by CD8$^+$ T cells in the absence of EBV-associated B-cell proliferative disorders

Newborn NOG mice were transplanted with hHSCs via intrahepatic injection to generate NOG-hCD34 mice. Twenty-eight NOG-hCD34 mice, which were reconstituted from 7 separate individual cord blood donors, respectively, were inoculated with EBV via an intravenous injection between 13 and 16 weeks after hHSC transplantation. Large amounts of EBV DNA were first detected at 3 wpi and then plateaued until 10 wpi, at which time, all mice were killed for analysis (Figure 1A). EBV infection was fatal for most mice, and 71.4% of the infected mice either died or were killed because

of severe weight loss by 10 wpi (Figure 1B). Interestingly, during 5-7 wpi, 20 male mice infected with EBV showed greater viremia and died more rapidly than 8 EBV-infected female mice (Figure 1C).

Yajima and colleagues[21] have previously reported that humanized NOG mice (hNOG mice) infected with EBV died within 10 wpi. In their study, infected hNOG mice exhibited tumors containing EBV-positive B cells, which is consistent with EBV-associated B-cell lymphomas.[21] Therefore, we first set forward to look for signs of B-cell proliferative disorders in PB and organs of EBV-infected NOG-hCD34 mice. As shown in Figure 1D, however, B-cell expansion in PB was not found after EBV infection, whereas expansion of $CD8^+$ T cells was observed. Gross examination of spleen and liver of EBV-infected mice showed hepatosplenomegaly (Figure 1E). MNCs were isolated from spleen, liver, ascitic lavage, BM, and kidneys, and the number of $CD19^+$ B cells and $CD8^+$ T cells were determined by flow cytometry. If the EBV-infected NOG-hCD34 mice had B-cell proliferative disorder, this analysis would show drastic increase of $CD19^+$ B cells rather than $CD8^+$ T cells. However, flow cytometry revealed systemic organ infiltration by $CD8^+$ T cells in infected mice, as shown by a 10-fold increase in spleen and BM and a 100-fold increase in liver, lung, kidney, and ascitic lavage (Figure 1F). In contrast, the only organ that showed a significant increase in the number of B cells in infected mice was liver (Figure 1F). Moreover, immunostaining showed that the infiltrating and/or expanded cells in spleen and liver of EBV-infected mice primarily consisted of $CD8^+$ T cells and $CD68^+$ histiocytes, with occasional $CD20^+$ B cells (Figure 1G), and that B-cell tumors in infected mice were not detected. Taken together, these findings are inconsistent with B-cell proliferative disorders in EBV-infected NOG-hCD34 mice.

It is well known that EBV-associated malignant B-cell lymphomas are infected with EBV.[1] To assess the presence of EBV-infected cells in infected mice, in situ hybridization for EBERs, which are viral RNAs expressed in all EBV-infected cells,[1] was applied. As shown in Figure 1H, EBER-positive cells were detected in both spleen and liver of infected mice. However, the frequency of EBER-positive cells ($< 1/20$ of infiltrating lymphocytes) was lower than previously reported.[21] This result provides additional evidence that the B-cell proliferation caused by EBV infection in our study was modest and negligible. Taken together, these results strongly suggest that the EBV-infected NOG-hCD34 mice in our study died in a manner distinctly different from EBV-associated B-cell lymphoma-dependent death.

Hemophagocytosis in BM, spleen, and liver of EBV-infected NOG-hCD34 mice

The expansion of and infiltration by $CD8^+$ T cells together with the large number of histiocytes in spleen and liver (Figure 1D,F,G) prompted us to look into the immunopathology for the cause of the high mortality. HLH is a fatal immunopathologic condition that can be caused by EBV infection, and infiltration of $CD8^+$ T cells into multiple organs and histiocyte proliferation are common in patients with EBV-HLH.[1,3,5,15] Cardinal laboratory findings for HLH include hemophagocytosis, cytopenia, hypercytokinemia, and hyperferritinemia.[3] To explore this possibility, we set out to examine the presence of hemophagocytosis in BM of infected mice by NSE staining. As observed in both the spleen and liver of infected mice (Figure 1G), a large number of granule-containing histiocytes was detected in BM (Figure 2A). In addition, Giemsa staining revealed that these histiocytes contained multiple intracellular erythrocytes (Figure 2B). However, granule-residing and/or hemophagocytosed histiocytes were scarcely detected in BM of mock-infected mice (data not shown).

H&E staining confirmed that a large number of histiocytes resided in spleen and hepatic sinusoids of infected mice compared with those of mock-infected mice (Figure 2C), which supports the immunostaining result (Figure 1G). Moreover, Berlin blue staining revealed that these histiocytes in spleen and hepatic sinusoids of infected mice contained intracellular hemosiderin, which was derived from engulfed erythrocytes (Figure 2D). Taken together, these results demonstrate the presence of prominent hemophagocytosis in BM, spleen, and hepatic sinusoids of EBV-infected NOG-hCD34 mice.

Normocytic anemia and thrombocytopenia in EBV-infected NOG-hCD34 mice

Cytopenia of more than 2 kinds of blood cells such as erythrocytes and platelets is one of the current diagnostic criteria for HLH.[3] To investigate whether cytopenia occurred in EBV-infected mice, the PB of 10 EBV-infected and 7 mock-infected mice was routinely analyzed. As shown in Figure 3B-E and also summarized in Table 1, we found that the numbers of erythrocytes and platelets, hematocrit level, and hemoglobin concentration decreased in PB of EBV-infected mice, suggesting erythropenia and thrombocytopenia. However, the values of MCV, MCH, and MCHC in PB of EBV-infected mice were comparable with those in mock-infected mice (Figure 3F-H). These results directly indicate that normocytic anemia occurred in EBV-infected NOG-hCD34 mice.

In addition to the normocytic anemia, viremia (Figure 3A) and leukocytosis (Figure 3I), which was predominantly $CD8^+$ T cells (Figure 1D), also were observed in EBV-infected mice. Moreover, EBV-infected mice eventually showed severe weight loss (Figure 3J). To assess the time course of pathologic events observed in EBV-infected mice, the obtained results from 10 EBV-infected mice were summarized in Table 1. Interestingly, leukocytosis was firstly observed after the appearance of viremia (1.60 ± 0.48 weeks after viremia). Then, erythropenia, thrombocytopenia, and a decrease in hemoglobin were followed by leukocytosis (1.88 ± 0.48 weeks, 2.13 ± 0.72 weeks, and 2.14 ± 0.46 weeks after viremia, respectively). Finally, weight loss was detected (2.89 ± 0.65 weeks after viremia). Taken together, these results suggest that the normocytic anemia in EBV-infected mice occurred after EBV replication and leukocytosis, ultimately leading to a morbid condition.

Organ infiltration and aberrant IFN-γ production by activated non-EBV–specific $CD8^+$ T cells

Because $CD8^+$ T-cell activation is thought to play an important role in HLH pathogenesis,[3-5] the activation status of $CD8^+$ T cells in infected mice was analyzed. As shown in Figure 4A, $CD8^+$ T cells dramatically increased in PB after EBV infection. This increase was attributed to the expansion of $CD45RO^+$ memory subsets, and, in particular, $CD45RO^+CD38^+HLA\text{-}DR^+$ activated subsets (Figure 4C-D). $CD45RA^+$ naive $CD8^+$ T cells displayed no increase after infection (Figure 4B). Moreover, the numbers of the activated $CD8^+$ T cells isolated from all analyzed organs of infected mice increased at least 10-fold compared with those of mock-infected mice (Figure 4E). Furthermore, splenic $CD8^+$ T cells were stained for Ki67, a nuclear antigen expressed exclusively in proliferating/activated cells.[32] As shown in Figure 4F, the percentage of splenic $CD8^+$ T cells positive for Ki67 in EBV-infected mice was approximately 2-fold greater than that in mock-infected mice.

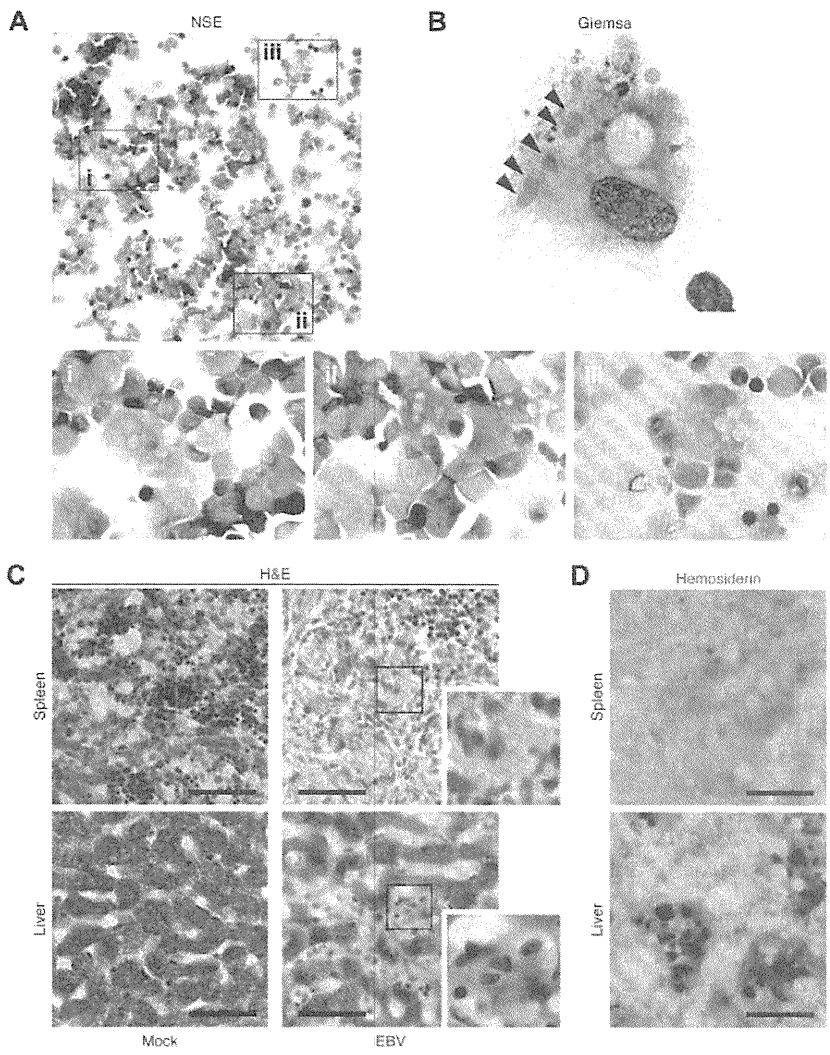

Figure 2. Hemophagocytosis in EBV-infected NOG-hCD34 mice. (A-B) Hemophagocytosis in the BM of EBV-infected mice. The specimens of the BM fluid smear of EBV-infected mice were prepared and assessed by NSE staining (A) and Giemsa staining (B). (A) NSE staining. Histiocytes (brown) and neutrophils (blue) were stained. Areas enclosed with squares (i-iii) indicate the histiocytes with granules and are, respectively, enlarged in panels i through iii. (B) Giemsa staining. A representative histiocyte with phagocytosis is shown. Arrowheads indicate engulfed erythrocytes. (C-D) Hemophagocytosis in the spleen and hepatic sinusoid of EBV-infected mice. Tissue sections were assessed by H&E staining (C) and Berlin blue staining (hemosiderin staining; D). (C) H&E staining. Representatives of spleen (top) and liver (bottom) of mock-infected mice (left) and EBV-infected mice (right) are shown. Areas enclosed with squares are enlarged in the bottom right of each panel and indicate morphologically activated histiocytes. (D) Berlin blue staining. Representatives of spleen (top) and liver (bottom) of EBV-infected mice are shown. Note that the cells stained with blue indicate hemosiderin-containing hemophagocytic histiocytes. Scale bars in panels C and D represent 50 μm.

Proinflammatory hypercytokinemia is another hallmark feature of HLH.[3] In addition, it is known that activated $CD8^+$ T cells can produce proinflammatory cytokines such as IFN-γ and TNF-α, which promote activation/proliferation of $CD8^+$ T cells and histiocytes.[3-6,12,13] To investigate this issue, the expression levels of IFNG (encodes IFN-γ) and TNFA (encodes TNF-α) in splenic $CD8^+$ T cells of EBV-infected and mock-infected mice were assessed. As shown in Figure 4G, IFNG was significantly elevated in $CD8^+$ T cells of infected mice, whereas TNFA was not. Next, the concentrations of IFN-γ and TNF-α in plasma were longitudinally assessed. A significant elevation of plasma IFN-γ concentration in infected mice was first detected at 4 wpi and was maintained at a high level (Figure 4H). In contrast, plasma TNF-α concentrations in infected mice were almost comparable with those in mock-infected mice (Figure 4I). Furthermore, to assess the dynamics of virus replication, $CD8^+$ T-cell activation, and IFN-γ hypercytokinemia in EBV-infected mice, the obtained results from 8 EBV-infected mice were summarized in Table 2. It is worth noting that the activation/expansion of $CD8^+$ T cells in PB and the elevation of plasma IFN-γ concentrations were first detected just after the appearance of viremia and occurred concurrently (0.38 ± 0.18 weeks and 0.50 ± 0.19 weeks after viremia, respectively). These findings suggest that $CD8^+$ T-cell activation and IFN-γ hypercytokinemia are elicited after EBV replication.

Because it has been known that EBV-specific HLA-restricted CTLs are easily induced by EBV infection,[1,33] the activation of $CD8^+$ T cells found in our EBV-infected mice may be because of a specific immune response against EBV antigens. To assess the immunologic specificity of the activated $CD8^+$ T cells against EBV, we isolated splenic human MNCs from 7 EBV-infected and 4 mock-infected mice. These mice underwent transplantation with hHSCs possessing HLA-A*2402 (supplemental Table 1), which is one of the dominant HLA class I alleles for EBV antigen presentation.[34] Specificity of the $CD8^+$ T cells for EBV antigens was evaluated by the use of HLA-A*2402 tetramers coupled with 5 different EBV peptides. HLA-A*2402 tetramers coupled with HIV-1 peptides were used as a negative control. As shown in Figure 4J, we detected HLA-A*2402–restricted EBV-specific $CD8^+$ T cells only in EBV-infected mice, although the frequency was quite low ($0.22\% \pm 0.09\%$).[33] However, HLA-A*2402–restricted HIV-1–specific $CD8^+$ T cells were not found (Figure 4J). These results suggest that the expansion of activated $CD8^+$ T cells was not directly because of EBV-specific antigen recognition.

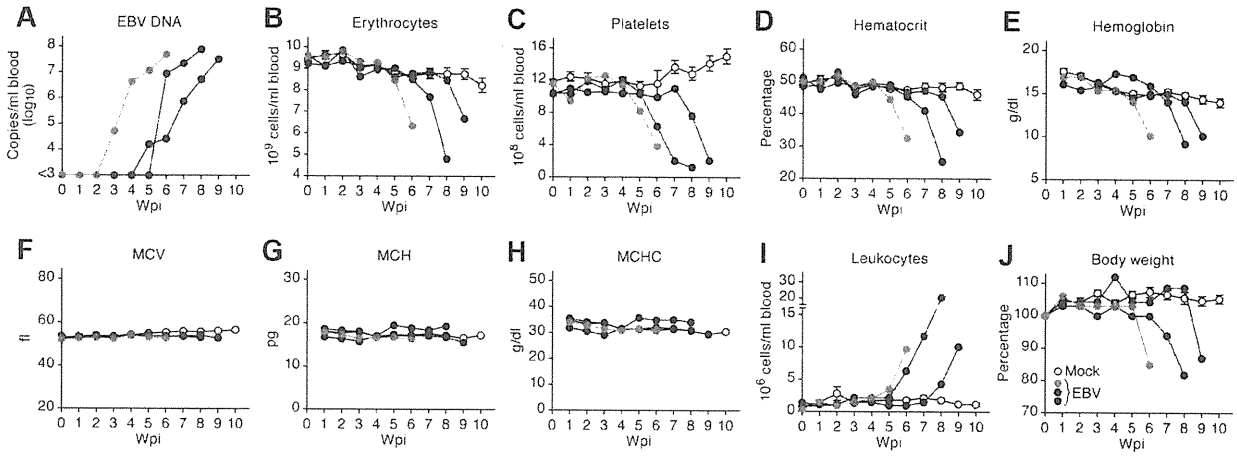

Figure 3. Viremia, normocytic anemia, thrombocytopenia, leukocytosis, and severe weight loss in EBV-infected NOG-hCD34 mice. (A) EBV load in the PB of 3 representative EBV-infected mice. (B-I) Longitudinal analyses of hematopoietic cells in PB. PB was routinely collected from mock-infected and EBV-infected mice, and the numbers of erythrocytes (B), platelets (C), and leukocytes (I) were measured by hematometry. Hematocrit (D), hemoglobin concentration (E), and the values of MCV (F), MCH (G), and MCHC (H) were also measured by hematometry. (J) Change on body weight. The body weights of mock-infected and EBV-infected mice were routinely measured and are shown as the ratio to the initial weight. Results from mock-infected mice (n = 7) are presented in means ± SEM, and representative results of 3 EBV-infected mice are, respectively shown. Each color represents the result from an identical EBV-infected mouse.

Relevance of EBV load, IFN-γ hypercytokinemia, and CD8$^+$ T-cell activation in respect to the morbid condition in EBV-infected NOG-hCD34 mice

It is known that EBV rarely infects T cells and can cause a T-cell proliferative disorder.[1,3,11,35] This disorder is known as chronic active EBV infection (CAEBV) and HLH can be accompanied by CAEBV.[1,3,11,35] To assess whether T cells are infected with EBV in NOG-hCD34 mice, splenic MNCs were sorted into human CD4$^+$, CD8$^+$, CD19$^+$, and murine CD45$^+$ fractions and the amount of EBV DNA in each fraction was quantified. When the murine CD45$^+$ fraction was used as the background control, no significant amount of EBV DNA was detected in human CD4$^+$ and CD8$^+$ fractions (Figure 5A). However, a large amount of EBV DNA (> 70 copies/cell) was detected in human CD19$^+$ B-cell fraction (Figure 5A). Although it is known that EBV infection in T cells induce the proliferation of the infected cell,[1,3,11,35] the number of EBER-positive cells was small (Figure 1H), and the level of viral DNA in either CD4$^+$ T cells or CD8$^+$ T cells was comparable with that of the background sample (Figure 5A). Therefore, these results suggest that the EBV-associated T-cell proliferative disorder is not likely caused in infected mice and that the pathogenesis observed in EBV-infected NOG-hCD34 mice is distinct from CAEBV-like disorder.

MNCs were isolated from spleen, liver, ascitic lavage, BM, and kidneys, and the amount of viral DNA was assessed. As shown in Figure 5B, large amounts of EBV DNA were detected in all organs assessed, showing systemic and productive replication of EBV. In addition, immunostaining revealed the expression of lytic viral proteins, ZEBRA (derived from bzlf1), and gp110 (derived from balf4), in both spleen and liver (Figure 5C). Moreover, RT-PCR revealed that not only latent viral genes (lmp1, lmp2a, and ebna2a) but also lytic viral genes (bzlf1, balf2, bxlf1, barf1, bclf1, and bllf1) were expressed in spleen of infected mice (Figure 5D). These results demonstrate that productive EBV replication takes place in infected NOG-hCD34 mice.

Clinical studies have shown that patients with EBV-HLH and a high viral load go on to have a worse prognosis than those with a

Table 1. Summary of the time points when hematologic disorders and severe weight loss were first observed*

Mouse no.†	VL‡	Leukocytosis§¶	Erythropenia§‖	Thrombocytopenia§‖	HGB decrease§‖	Weight loss§‖
Mouse 1	5	7 (+2)	6 (+1)	6 (+1)	6 (+1)	9 (+4)
Mouse 2	5	8 (+3)	9 (+4)	8 (+3)	9 (+4)	9 (+4)
Mouse 3	3	8 (+5)	–	9 (+6)	–	10 (+7)
Mouse 4	4	5 (+1)	6 (+2)	–	6 (+2)	–
Mouse 5	5	6 (+1)	6 (+1)	8 (+3)	8 (+3)	8 (+3)
Mouse 6	3	3 (± 0)	3 (± 0)	3 (± 0)	4 (+1)	4 (+1)
Mouse 7	3	5 (+2)	6 (+3)	6 (+3)	6 (+3)	6 (+3)
Mouse 8	4	5 (+1)	–	5 (+1)	–	5 (+1)
Mouse 9	6	6 (± 0)	7 (+1)	6 (± 0)	7 (+1)	7 (+1)
Mouse 10	7	8 (+1)	10 (+3)	–	–	9 (+2)
Average ± SEM**	–	1.60 ± 0.48	1.88 ± 0.48	2.13 ± 0.72	2.14 ± 0.46	2.89 ± 0.65

HGB indicates hemoglobin; VL, viral load; and wpi, weeks postinfection.
*The time points when infected mice showed significant differences to mock-infected mice are presented as wpi.
†The results from mice no. 2, 7, and 9 are shown in Figure 3.
‡The wpi when EBV DNA was firstly detected is presented.
§The values in parentheses represent the difference of each parameters to VL.
¶The wpi when the value was more than the average of mock-infected mice + SD is presented.
‖The wpi when the value was more than the average of mock-infected mice − SD is presented.
**The differences to VL (represented in parentheses) are summarized and presented as average ± SEM.

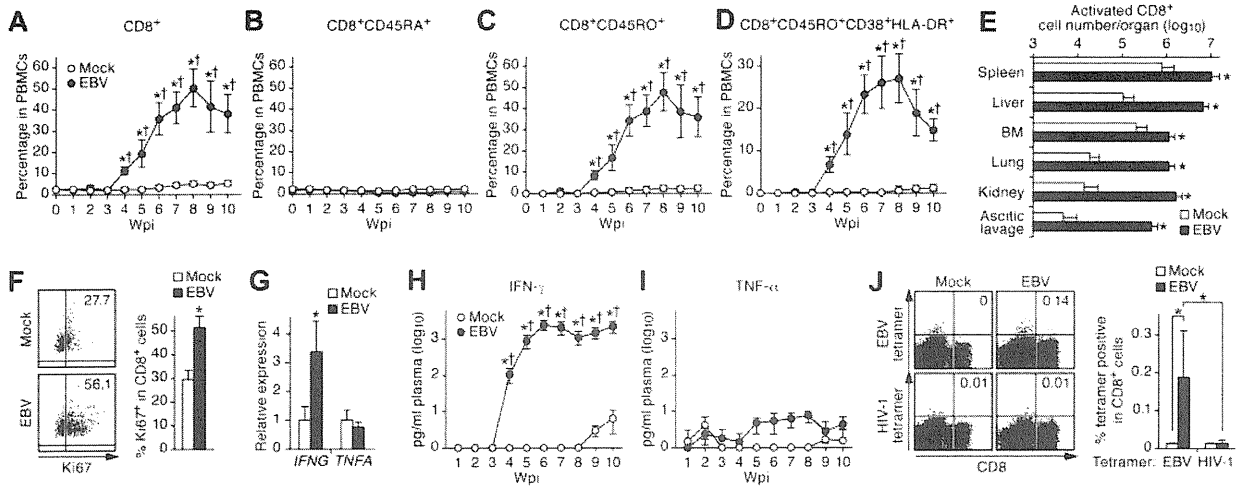

Figure 4. Expansion and activation of CD8+ T cells and IFN-γ hypercytokinemia in EBV-infected NOG-hCD34 mice. (A-D) Dynamics of human CD8+ T cells in PB. PB was routinely collected from mock-infected mice (n = 5) and EBV-infected mice (n = 12) and was analyzed by flow cytometry. Percentages of CD8+ cells (A), CD8+CD45RA+ cells (B), CD8+CD45RO+ cells (C), and CD8+CD45RO+CD38+HLA-DR+ cells (D) in PBMCs are, respectively shown. (E) Expansion of activated CD8+ T cells in multiple organs of EBV-infected mice. The cell numbers of CD8+CD45RO+CD38+HLA-DR+ cells (activated CD8+ T cells) in the spleen, liver, BM, lung, kidney, and ascitic lavage fluid of mock-infected mice (n = 4) and EBV-infected mice (n = 7) are shown. (F) Ki67 expression in CD8+ T cells. (Left) Representatives of splenic CD8+ T cells of mock-infected and EBV-infected mice. Values on quadrants represent the percentages of CD8+ T cells positive for Ki67. (Right) The percentages of Ki67+ cells in splenic CD8+ T cells of mock-infected mice (n = 4) and EBV-infected mice (n = 7) are shown. (G) mRNA expression in CD8+ T cells. Splenic CD8+ T cells of mock-infected mice (n = 6) and EBV-infected mice (n = 9) were isolated by cell sorting. The expression levels of *IFNG* (left) and *TNFA* (right) were analyzed by real-time RT-PCR and were normalized to that of *GAPDH*. Results are presented as the fold change compared with the value in mock-infected mice. (H-I) Longitudinal quantification of IFN-γ and TNF-α in plasma. Plasma was routinely collected from mock-infected mice (n = 4) and EBV-infected mice (n = 7), and the concentrations of IFN-γ (H) and TNF-α (I) were quantified by cytokine bead array system. (J) Detection of EBV-specific HLA-A*2402–restricted CD8+ cells. Splenic human MNCs isolated from mock-infected mice (n = 4) and EBV-infected mice (n = 7) were stained with an anti-CD8 antibody and either HLA-A*2402 EBV tetramers or HLA-A*2402 HIV-1 tetramers (as a negative control of the assay) and were analyzed by flow cytometry. Representatives (left) and the percentages of CD8+ T cells positive for the tetramers in mock-infected and EBV-infected mice (right) are shown. Asterisks in panels A, C, D, and H represent statistic significance ($P < .05$ by Student *t* test) versus the value obtained from the mock-infected mice, and daggers represent statistic significance ($P < .05$ by paired *t* test) vs the initial value. Asterisks in panel E represent statistic significance ($P < .05$ by Welch *t* test) versus the value obtained from the mock-infected mice. Asterisks in panel F, G, and J represent statistic significance ($P < .05$ by Student *t* test) versus the value obtained from the mock-infected mice.

low viral load.[4] To investigate whether the relevance between viral load and immune activation is observed in our model, we compared the level of EBV DNA and IFN-γ concentration in plasma and Ki67 expression in splenic CD8+ T cells to one another in each infected mouse. As shown in Figure 5E, the percentage of Ki67+ cells in splenic CD8+ T cells significantly correlated with the concentration of IFN-γ in plasma. In addition, we found that the EBV load in plasma positively and significantly correlated with both the percentage of splenic Ki67+CD8+ T cells (Figure 5F) and plasma IFN-γ concentration (Figure 5G). Moreover, the infected mice that were killed before 10 wpi because of severe weight loss tended to exhibit greater amounts of EBV DNA copies, IFN-γ concentrations, and Ki67 expression in CD8+ T cells than the infected mice that survived until 10 weeks (Figures 5E-G).

Table 2. Summary of the time points when immunologic disorders and severe weight loss were first observed*

Mouse no.	VL†	Activated CD8‡§	IFN-γ†¶	Weight loss§‖
Mouse 11	4	4 (± 0)	4 (± 0)	–
Mouse 12	4	4 (± 0)	4 (± 0)	6 (+2)
Mouse 13	3	4 (+1)	4 (+1)	6 (+3)
Mouse 14	4	4 (± 0)	4 (± 0)	9 (+5)
Mouse 15	3	3 (± 0)	4 (+1)	8 (+5)
Mouse 16	4	4 (± 0)	4 (± 0)	–
Mouse 17	3	4 (+1)	4 (+1)	6 (+3)
Mouse 18	3	4 (+1)	4 (+1)	5 (+2)
Average ± SEM**	–	0.38 ± 0.18	0.50 ± 0.19	3.33 ± 0.56

VL indicates viral load; and wpi, weeks postinfection.

*The time points when infected mice showed significant differences to mock-infected mice are presented as wpi.

†The wpi when EBV DNA was firstly detected is presented.

‡The values in parentheses represent the difference of each parameters to VL.

§The wpi when the parcentage CD8+CD45RO+CD38+HLA-DR+ cells in PBMCs of each infected mouse was more than the average of that of mock-infected mice + SD is presented.

¶The wpi when the concentration of IFN-γ in plasma of each infected mouse was more than the average of mock-infected mice + SD is presented.

‖The wpi when the value was more than the average of mock-infected mice − SD is presented.

**The differences to VL (represented in parentheses) are summarized and presented as average ± SEM.

Decrease in the number of natural killer cells, myeloid dendritic cells, and plasmacytoid dendritic cells in the spleen and EBER1 detection in the plasma of EBV-infected mice

To further investigate the dynamics of EBV-HLH–like disorders in infected mice, we assessed the proportion of human leukocytes in the spleen. As shown in Figure 6A, the numbers of naive, memory, and regulatory CD4+ T cells in the spleen of infected mice were comparable with those in mock-infected mice. However, we found a significant decrease in the number of natural killer (NK) cells, myeloid dendritic cells (MDCs), and plasmacytoid dendritic cells (PDCs) in the spleen of infected mice (Figure 6B-C). Moreover, we quantified the concentration of IFN-β in the plasma of infected mice and found that the level of IFN-β in infected mice was comparable with that in mock-infected mice (Figure 6D). Furthermore, the level of IFN-β in plasma did not correlate with the levels of EBV DNA, IFN-γ concentration, or Ki67 expression in CD8+ T cells (data not shown). These data suggest that IFN-β is not associated with the progression of the EBV-HLH–like disorder.

It was also reported that high levels of EBER1 were detected in plasma or sera of EBV-HLH patients.[31] We quantified the amount of EBER1 in the plasma of 14 infected mice and found that high

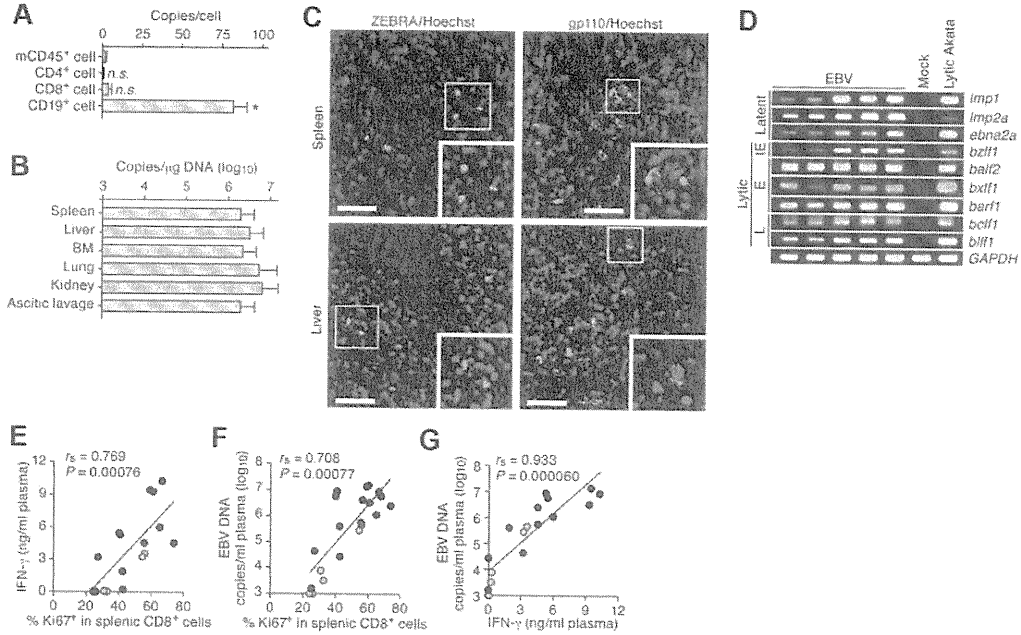

Figure 5. Productive EBV replication and the relevance between EBV infection and immune activation in infected NOG-hCD34 mice. (A) Distribution of EBV DNA in splenic human MNCs. Splenic MNCs were isolated from EBV-infected mice (n = 7), and human leukocytes ($CD4^+$, $CD8^+$, and $CD19^+$ cells, respectively) and murine $CD45^+$ leukocytes ($mCD45^+$ cells, as the background control) were separated by cell sorting. Results are presented in EBV copies per cell of each cell populations. Asterisk represents statistic significance ($P < .05$ by Student *t* test) versus the value obtained from $mCD45^+$ cells. n.s. indicates no statistical significance. (B) Systemic EBV replication in multiple organs. DNA was extracted from the human MNCs that were isolated from spleen, liver, BM, lung, kidney, and ascitic lavage fluid of EBV-infected mice (n = 7), and the copy number of EBV DNA was measured. (C) Immunostaining for ZEBRA and gp110. Representatives of spleen (top) and liver (bottom) of EBV-infected mice are shown. ZEBRA and gp110 were shown in green, and nuclei were shown in blue by staining with Hoechst. Areas enclosed with squares are enlarged in bottom right of each panel. Scale bars represent 50 μm. (D) Expression of EBV genes. RNA was extracted from splenic human MNCs of 5 EBV-infected mice, a mock-infected mouse, and anti-IgG–stimulated Akata cells ("Lytic Akata"), and the expression of EBV latent genes (*Imp1*, *Imp2a*, and *ebna2a*) and EBV lytic genes (*bzlf1*, *balf2*, *bxlf1*, *barf1*, *bclf1*, and *blff1*) was determined by RT-PCR. As the internal control, *GAPDH* expression was also determined. IE indicates immediate early gene; E, early genes; and L, late genes. (E-G) Correlation between viral load in plasma, activation frequency of $CD8^+$ T cells, and the level of IFN-γ in plasma. The percentage of $Ki67^+$ cells in splenic $CD8^+$ T cells (x-axis) and the concentration of IFN-γ in plasma (y-axis; E), the percentage of $Ki67^+$ cells in splenic $CD8^+$ T cells (x-axis) and EBV DNA copies in plasma (y-axis; F), and the concentration of IFN-γ in plasma (x-axis) and EBV DNA copies in plasma (y-axis; G) are, respectively shown. Red dots represent the results from the EBV-infected mice exhibited severe weight loss and were killed before 10 wpi (n = 13), whereas gray dots represent the results from the EBV-infected mice survived until 10 wpi (n = 5). The lines present exponential approximation. Spearman rank correlation coefficient (r_s) was adopted to determine statistically significant correlation between each value.

levels of EBER1 were detected in 8 infected mice (Figure 6E). Notably, the level of EBER1 in plasma of infected mice was almost comparable with or greater than that of patients.[31] However, the level of EBER1 in plasma did not correlate with disease severity and the clinical/laboratory features of disease (data not shown).

Discussion

To simulate EBV pathogenesis in vivo, several experimental animal models have been established.[36-41] In addition, hHSC-transplanted humanized mouse models have been used for EBV studies.[16-21] In this study, we established a novel humanized mouse model of EBV infection. NOG-hCD34 mice, which were newborn NOG mice transplanted with hHSCs, displayed a condition that has a different pathology from B-cell lymphomas when infected with EBV. Further investigations of EBV-infected NOG-hCD34 mice demonstrated the following: (1) hepatosplenomegaly; (2) $CD8^+$ T-cell activation and organ infiltration; (3) IFN-γ hypercytokinemia; (4) normocytic anemia; (5) thrombocytopenia; (6) histiocyte proliferation; and (7) hemophagocytosis in BM, spleen, and liver. These 7 features displayed by EBV-infected NOG-hCD34 mice are strongly indicative of EBV-HLH. To the best of our knowledge, this is the first report demonstrating the pathogenesis of EBV-HLH in an animal model. In addition to the establishment of a novel model for EBV-HLH, we also found a significant correlation between viral replication and hyperimmune activation in infected mice. Furthermore, a significant decrease of type I IFN-producing cells such as MDCs, PDCs, and NK cells was observed in spleen of infected mice. Taken together, these findings suggest that productive EBV replication induces hyperactivation of $CD8^+$ T cells, and that the breakdown of balanced immunity associates with disease progression.

Murine models of congenital HLH have shed light on the pathogenesis of this poorly understood disorder.[12,13] For instance, Prf knockout mice developed HLH after LCMV infection, resulting in the death of most infected mice.[12] Interestingly, the importance of $CD8^+$ T-cell activation and IFN-γ on the pathogenesis of HLH was also suggested in the same study.[12] As previously reported,[3-6,12,13] we found an augmented expression of IFNG in splenic $CD8^+$ T cells of EBV-infected mice. In addition, we found that the activation/expansion of $CD8^+$ T cells in PB and IFN-γ cytokinemia occurred concurrently in infected mice (Table 2), suggesting that $CD8^+$ T-cell activation and IFN-γ production take place in an orchestrated and synergistic manner in EBV-infected mice. After the expansion of $CD8^+$ T cells and IFN-γ hypercytokinemia, normocytic anemia and thrombocytopenia were subsequently observed (Table 1). In fact, it was reported that proinflammatory cytokines, including IFN-γ, have the potential to activate macrophages/histiocytes and trigger hemophagocytosis both in vitro[42] and in vivo.[8,33] Our results suggest that overproduced IFN-γ elicited histiocyte activation, leading to hemophagocytosis and

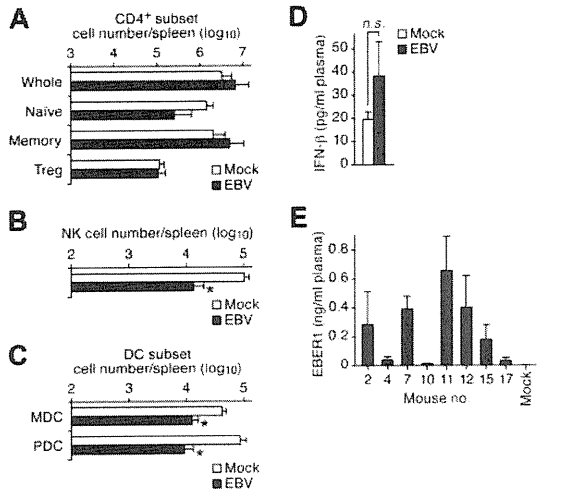

Figure 6. Decrease in the number of NK cells, MDCs, and PDCs and the detection of EBER1 and type I IFN in the plasma of infected NOG-hCD34 mice. (A-C) Human MNC numbers in spleen. The cell numbers of $CD4^+$ T-cell subset (whole, $CD4^+CD45^+$; naive, $CD4^+CD45RA^+CD45^+$; memory, $CD4^+CD45RO^+CD45^+$; Treg, $CD4^+FOXP3^+CD45^+$; A), NK cell ($CD56^+CD3^-CD45^+$; B), and DC subset (MDC, $Lineage^-[CD3^-CD14^-CD19^-CD56^-CD303^-]HLA\text{-}DR^{high}CD11c^{high}CD45^+$; PDC, $CD303^+CD45^+$; C) in spleen of mock-infected mice (n = 6) and EBV-infected mice (n = 6) are shown. Asterisks represent statistic significance ($P < .05$ by Welch t test) versus the value obtained from the mock-infected mice. (D) Quantification of IFN-β in plasma. The concentration of IFN-β in the plasma of mock-infected mice (n = 5) and EBV-infected mice (n = 14) was quantified by ELISA. n.s. indicates no statistical significance. (E) Quantification of EBER1 in plasma. The concentration of EBER1 in plasma of 8 EBV-infected mice and a mock-infected mouse was quantified as previously described.[31] The mouse numbers correspond with those in Tables 1 and 2.

anemia, and that $CD8^+$ T cells and IFN-γ played a pivotal role in promoting HLH.

In contrast to IFN-γ, type I IFNs (eg, IFN-β) are well-known to possess the robust potential to suppress virus replication, including EBV.[43] Recently, Iwakiri et al[31] have documented that EBER1 released from EBV-infected cells stimulates MDCs in a Toll-like receptor 3 (TLR3)–dependent manner and induces type I IFN production. In addition to MDCs, it was reported that NK cells also express TLR3 and are activated by TLR3 ligands.[44] Moreover, PDCs are involved in anti-EBV immunity by the secretion of type I IFN through TLR9 pathways.[43] These reports suggest that type I IFN produced by NK cells, MDCs, and PDCs through TLR3 and/or TLR9 signaling has the potential to suppress EBV-associated immunopathologic disorders. However, we found that NK cells, MDCs, and PDCs in the spleen of infected mice were severely decreased. Furthermore, we did not observe IFN-β hypercytokinemia in infected mice. These findings suggest that the depletion of type I IFN-producing cells such as NK cells, MDCs, and PDCs resulted in the absence of the induction of type I IFN production, which contributes to the progression of the EBV-HLH-like disorder in infected NOG-hCD34 mice.

Although the initial trigger of the $CD8^+$ T-cell activation causing the hyperimmune state in our EBV-infected mouse model remains unclear, several plausible explanations include direct and/or indirect $CD8^+$ T-cell activation by EBV-derived ligands. Reinforcing this assumption was our finding of a low frequency[33] of HLA-A*2402–restricted EBV-specific CTLs in the spleen of infected NOG-hCD34 mice, although their levels were comparable with previous reports.[18,20,21] In addition, TLR3 is expressed on $CD8^+$ T cells and induces a signaling cascade in these cells resulting in IFN-γ secretion without enhancing CTL activity.[45] As mentioned previously, EBER1 is able to trigger TLR3 signaling, and we detected high levels of EBER1 in the plasma of EBV-infected NOG-hCD34 mice at amounts comparable with EBV-infected patients (Figure 6E).[31] Therefore, it is possible that EBER1/TLR3 signaling in $CD8^+$ T cells may be one of the triggers to induce IFN-γ hypercytokinemia. Furthermore, when NOG-hCD34 mice were inoculated with heat-inactivated EBV, an absence of viremia, hyperimmune activation, anemia, and severe weight loss were observed (data not shown), suggesting that the agent(s) that triggered the hyperimmune activation in infected mice are derived from EBV replication. Moreover, we found that EBV DNA was detected in PB before $CD8^+$ T-cell activation and that the level of plasma EBV load positively correlated with the level of $CD8^+$ T-cell activation. In fact, a clinical study reported that EBV-HLH patients with a high viremia tend to exhibit a worse prognosis than those with a low viremia.[4] Therefore, our data suggest that productive EBV replication is essential for hyperactivation of $CD8^+$ T cells, which can lead to severe disorders.

In contrast to the EBV-infected humanized NOG mice displaying the EBV-HLH phenotype shown in our study, similar EBV-infected humanized NOG mice have exhibited EBV-associated B-cell proliferative disorders.[20,21] The different disease outcomes may be attributed to the different experimental approaches taken in conducting the studies. For instance, we used 20 male and 8 female NOG mice as hHSC recipients and found that the male mice exhibited higher levels of viremia and died more rapidly than female mice (Figure 1C). However, the previous studies used only female NOG mice as hHSC recipients.[20,21] Why male mice were more susceptible to a fatal outcome is unclear, however, a previous study has also observed a similar effect. Transgenic mice expressing hepatitis C virus core proteins had severe disorders and greater mortality in male transgenic mice compared with female transgenic mice.[46] Therefore, it is conceivable that the sex difference of the recipient NOG mice may be one of the underlying reasons why our findings varied from previous studies.[20,21] In addition, it was reported that their hNOG mice seem to have the potential to reproduce humoral immune responses against EBV[21] and HIV-1.[47] However, we have previously shown that our NOG-hCD34 mice were not capable of producing antibodies against HIV-1[25] and are unlikely to produce antibodies against EBV (data not shown). Thus, the difference in the potential of humoral immunity may also play a role in the EBV pathogenesis. Moreover, it is worth noting that EBV-HLH is a disease that tends to develop in children and young adults.[1,4] In this study, we transplanted hHSCs into newborn NOG mice and inoculated them with EBV at a relatively younger age period (13-16 weeks of age). However, the authors of the previous study used older NOG mice for hHSC transplantation and inoculated them with EBV at relatively older ages (20-38 weeks of age).[20,21] Because the age for EBV infection appears to be one of the critical determinants for the development of EBV-HLH in humans,[1,4] the difference in the age of humanized mice used for EBV infection may be a plausible explanation for the different pathologic outcomes caused by EBV infection. Overall, our system is more adept to simulate and reflect EBV-HLH pathogenesis in a manner relevant to what is observed humans compared with the previous study.

In conclusion, the model of acquired HLH we have generated in our humanized NOG mice will provide us with clues to elucidate how HLH is caused by EBV infection. Moreover, our model can also be used to develop and evaluate novel therapies targeting EBV-HLH. On the basis of not only on the current data, but on previous murine studies,[12,13] depletion of $CD8^+$ T cells as well as

neutralization of IFN-γ might prove useful in amelioration of disease. Furthermore, it will be interesting to evaluate the effects of B-cell–depleting antibodies on disease progression.

Acknowledgments

We thank Tomoko Kobayashi, Peter Gee, and Kenji Sugata (Institute for Virus Research, Kyoto University); Takeshi Sairenji (Tottori University); Hiroshi Kimura (Nagoya University Graduate School of Medicine); Kouichi Ohshima (School of Medicine, Kurume University); and Kinya Nagata (Bio Medical Laboratories Inc) for their generous help in our study. We would like to express our appreciation for Ms Kotubu Misawa's dedicated support.

This work was supported in part by Grants-in-Aid for Scientific Research (B21390137, S22220007 to Y.K.) from the Japan Society for the Promotion of Science; a Grant-in-Aid for Scientific Research on Priority Areas "Matrix of Infection Phenomena" (18073008 to Y.K.) from the Ministry of Education, Culture, Sports, Science and Technology of Japan; Research on Emerging and Re-emerging Infectious Diseases, and Research on HIV/AIDS from the Ministry of Health, Labor and Welfare of Japan; and the Naito Foundation (to Y.K.). K.S. was supported by Research Fellowships of the Japan Society for the Promotion of Science for Young Scientists.

Authorship

Contribution: K.S. and Y.K. designed the research; K.S., N.M., C.N., Y.S., D.I., R.T., and K.K. performed experiments; K.S., N.M., and M.I. constructed and maintained NOG-hCD34 mice; K.S., N.M., C.N., Y.S., D.I., M.M., R.T., and K.T. analyzed results; K.S. and C.N. designed the figures; and K.S., C.N., K.T., and Y.K. wrote the paper.

Conflict-of-interest disclosure: The authors declare no competing financial interests.

Correspondence: Yoshio Koyanagi, Laboratory of Virus Pathogenesis, Institute for Virus Research, Kyoto University, 53 Shogoinkawara-cho, Sakyo-ku, Kyoto, Kyoto 606-8507, Japan; e-mail: ykoyanag@virus.kyoto-u.ac.jp.

References

1. Rickinson AB, Kieff E. Epstein-Barr virus. In: Knipe DM, Howley PM, eds. *Fields Virology*. Vol. 2 (5th ed). Philadelphia, PA: Lippincott Williams & Wilkins; 2007:2655-2700.
2. Cohen JI. Epstein-Barr virus infections, including infectious mononucleosis. In: Braunwald E, Fauci AS, Kasper DL, et al, eds. *Harrison's Principals of Internal Medicine*. Vol. 1 (15th ed) New York, NY: McGraw-Hill; 2001:1109-1111.
3. Kasahara Y, Yachie A, Takei K, et al. Differential cellular targets of Epstein-Barr virus (EBV) infection between acute EBV-associated hemophagocytic lymphohistiocytosis and chronic active EBV infection. *Blood*. 2001;98(6):1882-1888.
4. Rouphael NG, Talati NJ, Vaughan C, Cunningham K, Moreira R, Gould C. Infections associated with haemophagocytic syndrome. *Lancet Infect Dis*. 2007; 7(12):814-822.
5. Su IJ, Chen RL, Lin DT, Lin KS, Chen CC. Epstein-Barr virus (EBV) infects T lymphocytes in childhood EBV-associated hemophagocytic syndrome in Taiwan. *Am J Pathol*. 1994;144(6):1219-1225.
6. Créput C, Galicier L, Buyse S, Azoulay E. Understanding organ dysfunction in hemophagocytic lymphohistiocytosis. *Intensive Care Med*. 2008; 34(7):1177-1187.
7. Janka GE. Hemophagocytic syndromes. *Blood Rev*. 2007;21(5):245-253.
8. Stepp SE, Dufourcq-Lagelouse R, Le Deist F, et al. Perforin gene defects in familial hemophagocytic lymphohistiocytosis. *Science*. 1999; 286(5446):1957-1959.
9. Coffey AJ, Brooksbank RA, Brandau O, et al. Host response to EBV infection in X-linked lymphoproliferative disease results from mutations in an SH2-domain encoding gene. *Nat Genet*. 1998; 20(2):129-135.
10. Rigaud S, Fondaneche MC, Lambert N, et al. XIAP deficiency in humans causes an X-linked lymphoproliferative syndrome. *Nature*. 2006; 444(7115):110-114.
11. Dupré L, Andolfi G, Tangye SG, et al. SAP controls the cytolytic activity of CD8+ T cells against EBV-infected cells. *Blood*. 2005;105(11):4383-4389.
12. Jordan MB, Hildeman D, Kappler J, Marrack P. An animal model of hemophagocytic lymphohistiocytosis (HLH): CD8+ T cells and interferon gamma are essential for the disorder. *Blood*. 2004;104(3):735-743.
13. Wu C, Nguyen KB, Pien GC, et al. SAP controls T cell responses to virus and terminal differentiation of TH2 cells. *Nat Immunol*. 2001;2(5):410-414.
14. Brown DE, McCoy MW, Pilonieta MC, Nix RN, Detweiler CS. Chronic murine typhoid fever is a natural model of secondary hemophagocytic lymphohistiocytosis. *PLoS ONE*. 2010;5(2):e9441.
15. Risdall RJ, McKenna RW, Nesbit ME, et al. Virus-associated hemophagocytic syndrome: a benign histiocytic proliferation distinct from malignant histiocytosis. *Cancer*. 1979;44(3):993-1002.
16. Islas-Ohlmayer M, Padgett-Thomas A, Domiati-Saad R, et al. Experimental infection of NOD/SCID mice reconstituted with human CD34+ cells with Epstein-Barr virus. *J Virol*. 2004;78(24):13891-13900.
17. Melkus MW, Estes JD, Padgett-Thomas A, et al. Humanized mice mount specific adaptive and innate immune responses to EBV and TSST-1. *Nat Med*. 2006;12(11):1316-1322.
18. Strowig T, Gurer C, Ploss A, et al. Priming of protective T cell responses against virus-induced tumors in mice with human immune system components. *J Exp Med*. 2009;206(6):1423-1434.
19. Traggiai E, Chicha L, Mazzucchelli L, et al. Development of a human adaptive immune system in cord blood cell-transplanted mice. *Science*. 2004; 304(5667):104-107.
20. Yajima M, Imadome K, Nakagawa A, et al. T cell-mediated control of Epstein-Barr virus infection in humanized mice. *J Infect Dis*. 2009;200(10):1611-1615.
21. Yajima M, Imadome KI, Nakagawa A, et al. A new humanized mouse model of Epstein-Barr virus infection that reproduces persistent infection, lymphoproliferative disorder, and cell-mediated and humoral immune responses. *J Infect Dis*. 2008;198(5):673-682.
22. Ito M, Hiramatsu H, Kobayashi K, et al. NOD/SCID/gammacnull mouse: an excellent recipient mouse model for engraftment of human cells. *Blood*. 2002;100(9):3175-3182.
23. Nie C, Sato K, Misawa N, et al. Selective infection of CD4+ effector memory T lymphocytes leads to preferential depletion of memory T lymphocytes in R5 HIV-1-infected humanized NOD/SCID/IL-2Rgammanull mice. *Virology*. 2009;394(1):64-72.
24. Sato K, Izumi T, Misawa N, et al. Remarkable lethal G-to-A mutations in vif-proficient HIV-1 provirus by individual APOBEC3 proteins in humanized mice. *J Virol*. 2010;84(18):9546-9556.
25. Sato K, Nie C, Misawa N, Tanaka Y, Ito M, Koyanagi Y. Dynamics of memory and naive CD8+ T lymphocytes in humanized NOD/SCID/IL-2Rgammanull mice infected with CCR5-tropic HIV-1. *Vaccine*. 2010;28(suppl 2):B32-37.
26. Shimizu N, Yoshiyama H, Takada K. Clonal propagation of Epstein-Barr virus (EBV) recombinants in EBV-negative Akata cells. *J Virol*. 1996; 70(10):7260-7263.
27. Sato K, Aoki J, Misawa N, et al. Modulation of human immunodeficiency virus type 1 infectivity through incorporation of tetraspanin proteins. *J Virol*. 2008;82(2):1021-1033.
28. Sato K, Yamamoto SP, Misawa N, Yoshida T, Miyazawa T, Koyanagi Y. Comparative study on the effect of human BST-2/Tetherin on HIV-1 release in cells of various species. *Retrovirology*. 2009;6:53.
29. Miura Y, Misawa N, Maeda N, et al. Critical contribution of tumor necrosis factor-related apoptosis-inducing ligand (TRAIL) to apoptosis of human CD4+ T cells in HIV-1–infected hu-PBL-NOD-SCID mice. *J Exp Med*. 2001;193(5):651-659.
30. Jebbink J, Bai X, Rogers BB, Dawson DB, Scheuermann RH, Domiati-Saad R. Development of real-time PCR assays for the quantitative detection of Epstein-Barr virus and cytomegalovirus, comparison of TaqMan probes, and molecular beacons. *J Mol Diagn*. 2003;5(1):15-20.
31. Iwakiri D, Zhou L, Samanta M, et al. Epstein-Barr virus (EBV)-encoded small RNA is released from EBV-infected cells and activates signaling from Toll-like receptor 3. *J Exp Med*. 2009;206(10): 2091-2099.
32. Iatropoulos MJ, Williams GM. Proliferation markers. *Exp Toxicol Pathol*. 1996;48(2-3):175-181.
33. Hislop AD, Taylor GS, Sauce D, Rickinson AB. Cellular responses to viral infection in humans: lessons from Epstein-Barr virus. *Annu Rev Immunol*. 2007;25:587-617.
34. Rickinson AB, Moss DJ. Human cytotoxic T lymphocyte responses to Epstein-Barr virus infection. *Annu Rev Immunol*. 1997;15:405-431.
35. Kimura H. Pathogenesis of chronic active Epstein-Barr virus infection: is this an infectious disease, lymphoproliferative disorder, or immunodeficiency? *Rev Med Virol*. 2006;16(4):251-261.
36. Epstein MA, Hunt RD, Rabin H. Pilot experiments with EB virus in owl monkeys (Aotus trivirgatus). I Reticuloproliferative disease in an inoculated animal. *Int J Cancer*. 1973;12(2):309-318.

37. Epstein MA, Rabin H, Ball G, Rickinson AB, Jarvis J, Melendez LV. Pilot experiments with EB virus in owl monkeys (Aotus trivirgatus). II. EB virus in a cell line from an animal with reticuloproliferative disease. *Int J Cancer.* 1973;12(2):319-332.

38. Mosier DE. Immunodeficient mice xenografted with human lymphoid cells: new models for in vivo studies of human immunobiology and infectious diseases. *J Clin Immunol.* 1990;10(4):185-191.

39. Shope T, Dechairo D, Miller G. Malignant lymphoma in cottontop marmosets after inoculation with Epstein-Barr virus. *Proc Natl Acad Sci U S A.* 1973;70(9):2487-2491.

40. Takashima K, Ohashi M, Kitamura Y, et al. A new animal model for primary and persistent Epstein-Barr virus infection: human EBV-infected rabbit characteristics determined using sequential imaging and pathological analysis. *J Med Virol.* 2008; 80(3):455-466.

41. Wedderburn N, Edwards JM, Desgranges C, Fontaine C, Cohen B, de Thé G. Infectious mononucleosis-like response in common marmosets infected with Epstein-Barr virus. *J Infect Dis.* 1984; 150(6):878-882.

42. van Lier RA, ten Berge IJ, Gamadia LE. Human CD8+ T-cell differentiation in response to viruses. *Nat Rev Immunol.* 2003;3(12):931-939.

43. Lim WH, Kireta S, Russ GR, Coates PT. Human plasmacytoid dendritic cells regulate immune responses to Epstein-Barr virus (EBV) infection and delay EBV-related mortality in humanized NOD-SCID mice. *Blood.* 2007;109(3):1043-1050.

44. Schmidt KN, Leung B, Kwong M, et al. APC-independent activation of NK cells by the Toll-like receptor 3 agonist double-stranded RNA. *J Immunol.* 2004;172(1):138-143.

45. Tabiasco J, Devevre E, Rufer N, et al. Human effector CD8+ T lymphocytes express TLR3 as a functional coreceptor. *J Immunol.* 2006;177(12): 8708-8713.

46. Moriya K, Fujie H, Shintani Y, et al. The core protein of hepatitis C virus induces hepatocellular carcinoma in transgenic mice. *Nat Med.* 1998;4(9):1065-1067.

47. Watanabe S, Terashima K, Ohta S, et al. Hematopoietic stem cell-engrafted NOD/SCID/IL2Rgammanull mice develop human lymphoid systems and induce long-lasting HIV-1 infection with specific humoral immune responses. *Blood.* 2007;109(1):212-218.

Establishment of a xenograft model of human myelodysplastic syndromes

Yukari Muguruma,[1] Hiromichi Matsushita,[1,2] Takashi Yahata,[1,3] Shizu Yumino,[1] Yumiko Tanaka,[2] Hayato Miyachi,[2] Yoshiaki Ogawa,[4] Hiroshi Kawada,[4] Mamoru Ito,[5] and Kiyoshi Ando[1,4]

[1]Research Center for Regenerative Medicine, Division of Hematopoiesis, Tokai University School of Medicine, Japan; [2]Department of Laboratory Medicine, Tokai University School of Medicine, Japan; [3]Department of Cell Transplantation, Tokai University School of Medicine, Japan; [4]Department of Hematology and Oncology, Tokai University School of Medicine, Japan; [5]Central Institute of Experimental Animals, Japan

Funding: this work was supported by grants to KA and YM, a Research Grant of the Scientific Frontier Program a Basic Research Grant from the Ministry of Education, Culture, Sports, Science and Technology of Japan.

Acknowledgments: the authors would thank members of the animal facility of Tokai University for their care of animals and all members of the Research Center for Regenerative Medicine for their support.

Manuscript received May 10, 2010. Revised version arrived on November 29, 2010. Manuscript accepted on December 24, 2010.

Correspondence:
Kiyoshi Ando, Department of Hematology and Oncology, Tokai University School of Medicine, 143 Shimokasuya, Isehara, 259-1193, Japan.
E-mail: andok@keyaki.cc.u-tokai.ac.jp

The online version of this article has a Supplementary Appendix.

ABSTRACT

Background
To understand how myelodysplastic syndrome cells evolve from normal stem cells and gain competitive advantages over normal hematopoiesis, we established a murine xenograft model harboring bone marrow cells from patients with myelodysplastic syndromes or acute myeloid leukemia with myelodysplasia-related changes.

Design and Methods
Bone marrow $CD34^+$ cells obtained from patients were injected, with or without human mesenchymal stem cells, into the bone marrow of non-obese diabetic/severe combined immunodeficient/IL2R ^{null} hosts. Engraftment and differentiation of cells derived from the patients were investigated by flow cytometry and immunohistochemical analysis.

Results
Co-injection of patients' cells and human mesenchymal stem cells led to successful engraftment of patient-derived cells that maintained the immunophenotypes and genomic abnormalities of the original patients. Myelodysplastic syndrome-originated clones differentiated into mature neutrophils, megakaryocytes, and erythroblasts. Two of the samples derived from patients with acute myeloid leukemia with myelodysplasia-related changes were able to sustain neoplastic growth into the next generation while these cells had limited differentiation ability in the murine host. The hematopoiesis of mice engrafted with patients' cells was significantly suppressed even when human cells accounted for less than 1% of total marrow mononuclear cells. Histological studies revealed invasion of the endosteal surface by patient-derived $CD34^+$ cells and disruption of extracellular matrix architecture, which probably caused inhibition of murine hematopoiesis.

Conclusions
We established murine models of human myelodysplastic syndromes using cells obtained from patients: the presence of neoplastic cells was associated with the suppression of normal host hematopoiesis. The efficiency of engraftment was related to the presence of an abnormality in chromosome 7.

Key words: xenograft, MDS, NOG mouse, niche, MSC.

Citation: Muguruma Y, Matsushita H, Yahata T, Yumino S, Tanaka Y, Miyachi H, Ogawa Y, Kawada H, Ito M, and Ando K. Establishment of a xenograft model of human myelodysplastic syndromes. Haematologica 2011;96(4):543-551. doi:10.3324/haematol.2010.027557

Introduction

Myelodysplastic syndromes (MDS) are a heterogeneous group of clonal hematopoietic disorders originating from primitive hematopoietic cells and some of the least studied hematopoietic malignancies due largely to difficulties in creating an *in vivo* model suitable for studying the biology of MDS since these syndromes cause variable degrees of morphological dysplasia in non-lymphoid lineages and accompanying hematopoietic failure.[1,2] The prognosis of MDS patients is generally poor with an approximately 25% risk of the disease evolving into acute myeloid leukemia (AML).[3] A wide variety of cytogenetic abnormalities is recognized in nearly half of MDS patients.[4,5] Although a multi-step process of disease development has been proposed,[6-9] the current understanding of the molecular pathogenesis of this disease is limited and, consequently, the precise mechanisms of how MDS cells evolve from normal hematopoietic cells remain unclear.

Mouse models of human diseases have been proven to be useful tools for elucidating the biology of various diseases and for evaluating the efficacy of evolving therapy.[10] The successful establishment of murine xenograft models for human AML has yielded empirical evidence for the existence of so-called 'cancer stem cells', a minor subpopulation of cells responsible for maintenance of neoplastic proliferation.[11-13] In addition, recent studies demonstrated that chemotherapy-resistant leukemic stem cells reside in the endosteal region of bone marrow.[14,15] These findings helped to clarify how acute leukemia cells are maintained and propagated *in vivo*; however, little is known about the behavior of MDS cells in the bone marrow microenvironment partly because of the difficulties in obtaining a suitable *in vivo* model for this disease. The reason for the selective outgrowth of MDS clones and the concurrent decrease in normal hematopoietic stem cells in patients does, therefore, remain elusive.

To establish a murine model of human MDS, which would undoubtedly be of benefit in the study of the pathology and biology of MDS, we transplanted bone marrow $CD34^+$ cells from patients with MDS and acute myeloid leukemia with myelodysplasia-related changes (AML-MRC) and human mesenchymal stem cells (MSC) as auxiliary cells in murine bone marrow using an established intramedullary co-transplantation method.

Design and Methods

Patients and preparation of human cells

The experimental protocol of this study was approved by the Institutional Review Board of Tokai University, School of Medicine, and all human samples were handled accordingly. Bone marrow samples were obtained from six patients with MDS, eight patients with AML-MRC, and four healthy individuals after obtaining written informed consent. The clinical characteristics and immunophenotypes of the patients are summarized in *Online Supplementary Tables S1 and S2*, respectively. $CD34^+$ cells were selected using the CD34 Progenitor Cell Isolation Kit (Miltenyi Biotec, Sunnyvale, CA, USA) according to the manufacturer's instructions as described previously.[16] The purity of the selected bone marrow CD34+ cells was always more than 95%. Human MSC were purchased from Lonza Walkersville Inc. (Walkersville, MD, USA) and cultured according to the directions supplied by the company. In some experiments, MSC were established from the $CD34^-$ fraction of patients' cells. The ability of the cells to differentiate into adipocytes, chondrocytes and osteoblasts was assessed and confirmed *in vitro* as described previously[17] before the cells were used for this study (*data not shown*).

Antibodies

The following monoclonal antibodies were used for flow cytometry: anti-CD7 (4H9), -CD11b (D12), -CD13 (L138), -CD14 (M P9), -CD19 (SJ25C1), -CD36 (CB38(NL07)), -CD38 (HB7), -CD56 (MY31), -CD61 (VI-PL2), -CD64 (10.1), and -HLA-DR (L243, all from BD Biosciences, San Jose, CA, USA); anti-CD33 (WM53), -CD34 (581), -CD41b (P2), -CD45 (J.33), and CD117 (95C3, all from Coulter/Immunotech, Marseille, France); and MPO (MPO-7, DACO, Denmark).

The following antibodies were used for tissue immunostaining: anti-CD15 (80H5, 1:150, Coulter/Immunotech); anti-CD31 (1:100, TECNE Corporation, Minneapolis, MN, USA); anti-CD34 (My10, 1:20), -CD45 (2D1, 1:200), and -CD38 (HIT2, 1:100, all from BD Biosciences); anti-glycophorin A (JC159, 1:400) and -CD61(Y2/51, 1:1000, both from DACO); anti-fibronectin (1:400, Sigma, St Louis, MO, USA); and anti-PCNA (1:200, abcam, Cambridge, UK).

Experimental animals, lentiviral gene transduction, and cell transplantation

Non-obese diabetic/severe combined immunodeficient/IL2R ^{null} (NOG) mice were maintained in sterile microisolator cages in the animal facility of Tokai University School of Medicine. The mice were irradiated with 250 cGy from an X-ray irradiator (HW-300, Hitex, Osaka, Japan) 24 h prior to intramedullary transplantation of cells. All procedures were approved by the Animal Care Committee of Tokai University. The MSC were transduced with the *GFP* gene as described previously.[17]

Analysis of human cells

The mice were killed humanely 8 to 16 weeks after transplantation, and the entire bone marrow contents of the injected tibiae were collected in phosphate-buffered saline containing 0.5% bovine serum albumin and 0.5 M EDTA. The total number of bone marrow mononuclear cells was counted for each bone of individual experimental animals. The number of non-human bone marrow cells was obtained by calculation. Aliquots of cells were used to examine the percentages of cells expressing human cell surface antigens. A four-color flow cytometric analysis was conducted using FACSCaliber. Quadrants were set to include at least 97% of the isotype-negative cells. The proportion of each lineage was calculated from 10,000 events acquired using the CELLQuest software package. The remaining cells were saved for secondary transplantation, cytospin preparation for morphological examination, chromosomal analysis and fluorescence *in situ* analysis (FISH). Chromosomal analysis was conducted using a conventional method in the clinical laboratory of the University Hospital, while the FISH analysis was performed at SRL Inc. (Tokyo, Japan). The preparation of the bone marrow for histological studies, immunofluorescent staining and enzyme immunohistochemistry were performed as described previously.[18] Images of stained slides were captured using an LSM510 META confocal microscope with a 63X/1.2 numeric aperture c-Apochromat objective lens (Carl Zeiss, Jena, Germany) and an Olympus Ax80 microscope with a 20X/0.70 numeric aperture UplanApo lens equipped with a DP71 digital camera (Olympus, Japan). Images were transferred to Adobe Photoshop CS4 (Adobe Systems, San Jose, CA, USA)

Histological analysis of bone

For serial transplantation experiments, the percentage of cells in the endosteal region (within 5 cells' distance) was obtained by

counting the cells in the entire field of bone specimens under the light field microscope. More than five slides were examined for each transplant.

Statistics

Data are presented as the mean ± standard deviation. The two-sided *P* value was determined by testing the null hypothesis that the two population medians are equal. *P* values less than 0.05 were considered to be statistically significant.

Results

Engraftment of myelodysplastic syndrome-originated human hematopoietic cells in murine bone marrow

We previously reported that intramedullary injection of cord blood hematopoietic stem cells along with human MSC improved engraftment of human cells in the murine microenvironment.[18] We, therefore, transplanted bone marrow CD34$^+$ cells, which included hematopoietic stem cells and primitive progenitors, obtained from six patients with MDS, eight patients with AML-MRC and four healthy individuals, into the bone marrow of NOG mice with or without human MSC. Flow cytometric analysis detected the presence of human CD45$^+$ cells, at varying frequencies, in the bone marrow of 8/8, 12/23, and 4/4 recipient mice injected with bone marrow CD34$^+$ cells from the MDS patients, the AML-MRC patients, and the healthy individuals, respectively (Table 1). As expected, transplantation of MSC alone did not result in hematopoietic engraftment (*data not shown*). Further lineage analysis revealed a CD33$^+$ myeloid dominant differentiation, 60% or more, in three of six MDS cases (3/8 mice engrafted) and three of eight AML-MRC cases (9/12 mice engrafted), suggesting the engraftment of MDS-originated cells (Table 1; patients 2, 5, 6, 11, 13, and 14, and Figure 1A). Human cells recovered from transplanted animals were positive for cell surface markers found on the original patients' cells (*Online Supplementary Table S2*), such as CD13 (74.90%) and CD56 (32.08%) for patient 11, CD7 (72.13%) and CD41b (60.12%) for patient 13, and CD13 (81.92%, 37.86% of which co-expressed CD34) and CD117 (31.41%) for patient 14.

To confirm that this was indeed engraftment of MDS-originated cells, we performed cytogenetic and morphological analyses on human cells recovered from the mice engrafted with patients' bone marrow cells. FISH analysis confirmed cytogenetic abnormalities of original bone marrow in the human cells isolated from mice engrafted with cells from patients 6, 11, and 13 (Figure 1B and *Online Supplementary Table S3*) in 100% of the cells analyzed. In addition, patient-specific chromosomal abnormalities (monosomy 7 for patient 13 and isochromosome 17 for patient 14) were detected in 100% of cells analyzed (Figure 1C). Morphological observations of cytospin samples and bone marrow histology of mice engrafted with bone marrow cells from patients 2 and 11 showed dysplа-

Table 1. Engraftment of bone marrow CD34$^+$ cells obtained from MDS and AML-MRC patients.

Patient N.	N. of injected cells, x10^4*	Auxiliary cells	# of mice engrafted/ injected	N. of cells recovered, x10^5 /tibia	Percentage of human cells	Percentages of CD34$^+$ cells in human cells†	Percentages of lineage cells in human cells†	
							CD33$^+$	CD19$^+$
1	23.7	allo	1/1	6.8	67.65	10.45	10.8	82.3
2	33.9	allo	1/1	4.0	88.92	39.71	67.37	21.17
3	32.4	allo	1/1	3.0	3.93	9.26	4.4	85.72
4	28.2	allo	1/1	2.18	0.48	9.94	0	95.47
5	40	auto	1/1	3.4	1.95	83.59	96.02	0
		dermal fibroblasts	1/1	2.7	0.83	27.71	51.81	49.13
		-	1/1	4.8	0.36	50.0	57.14	23.81
6	14	allo	1/1	1.6	0.15	8.43	88.0	0
7	236	allo	1/1	5.5	3.18	5.77	2.57	91.32
8	39	allo	0/1	4.8	0	NT	NT	NT
9	100	allo	1/1	6.3	0.14	10.67	7.25	79.81
10	500	allo	1/1	12.0	12.42	9.58	3.15	83.99
11	100	auto	1/1	4.8	0.32	20.59	95.52	3.96
		allo	1/1	0.67	3.28	8.03	86.22	0.71
	138	auto	2/2	3.4, 5.2	7.72, 1.14	28.19, 12.3	80.76,91.54	0.0, 8.0
		CD34$^-$ fraction	0/2	5.8, 6.2	0	NT	NT	NT
		-	1/1	4.8	0.49	13.46	60.0	29.09
12	250-1000	allo, auto	0/6	4.4-9.8	0	NT	NT	NT
	1000	-	0/2	6.9, 7.8	0	NT	NT	NT
13	500	allo	1/1	2.7	10.27	35.71	94.78	1.01
14	400	allo	1/1	0.45	89.29	36.10	80.69	0.73
		auto	2/2	0.63, 0.42	71.06, 83.4	35.74, 28.61	73.68, 90.20	0.24, 0.22
Normal individuals	5, 10, 7.8, 10	allo, auto	4/4	7.0, 3.8, 5.7, 14.7	32.7,2.9,45.5,12.8	8.7,16.2,6.7,8.5	5.9,18.6,7.7,15.1	76.9,71.4,72.9,67.1

*Auto indicates autologous MSC; allo, allogeneic MSC; -, not applicable; NT, not tested. *Indicated numbers of bone marrow CD34$^+$ cells were transplanted with or without 5~15 10^5 auxiliary cells. †Shown here are percentages of cell surface marker expressing cells in the human CD45$^+$ gate.*

sia typically associated with MDS, such as bi-nucleated myelocytes and megakaryocytes with separated nuclei (Figures 1D and 2A, and *data not shown*). In samples prepared with cells recovered from mice engrafted with bone marrow cells from patient 2, myelocytes with variable degrees of normal differentiation were easily seen, but there were also sporadic cells with dysplasia which were not seen in samples from animals engrafted with normal human bone marrow cells. Large blastic cells were prominent in cytospin samples of bone marrow cells prepared from mice engrafted with cells from patients 13 and 14 (Figure 1D and *data not shown*). Considering these findings collectively, mice injected with bone marrow cells from patients 2, 5, 6, 11, 13, and 14 were engrafted with MDS-originated cells. Five of these patients harbored one or more genetic abnormalities, most of which were abnormalities in chromosome 7 (*Online Supplementary Table S1*). In contrast, human cell engraftment of mice transplanted with cells obtained from normal individuals and patients 1, 3, 4, 7, 9, and 10 consisted mainly of B-lineage cells, typical of normal human cell differentiation in the NOG mice environment.[19-21] Analyses of cytospin samples prepared from human cells recovered from the bone marrow of these mice confirmed a B-cell dominant differentiation (Figure 1D). In addition, no clonal markers specific to patients' phenotype were detected by FISH analysis (*Online Supplementary Table S3*, patients 9 and 10). The human engraftment in mice injected with cells from these patients was, therefore, considered to come from a minor population of normal hematopoietic stem cells co-existing in the patients' bone marrow CD34$^+$ cells.

Co-transplantation of bone marrow CD34$^+$ cells along with human MSC facilitated the engraftment of MDS-originated cells (Table 1; patients 5 and 11). In mice transplanted with bone marrow CD34$^+$ cells and MSC, more than 80% of human cells expressed CD33 while less than 4% expressed CD19 (5/5), in contrast to the mice transplanted with bone marrow CD34$^+$ cells alone (23.81% and 29.09% CD19$^+$ cells) or in combination with dermal fibroblasts (49.13% CD19$^+$ cells) in which B-cell proliferation was more notable (3/3), thus suggesting that normal human cells were also engrafted. The co-injection of the CD34$^-$ fraction of bone marrow cells did not yield any human cell engraftment (2/2). These results indicate the unique property of MSC of facilitating the engraftment of MDS-originated cells.

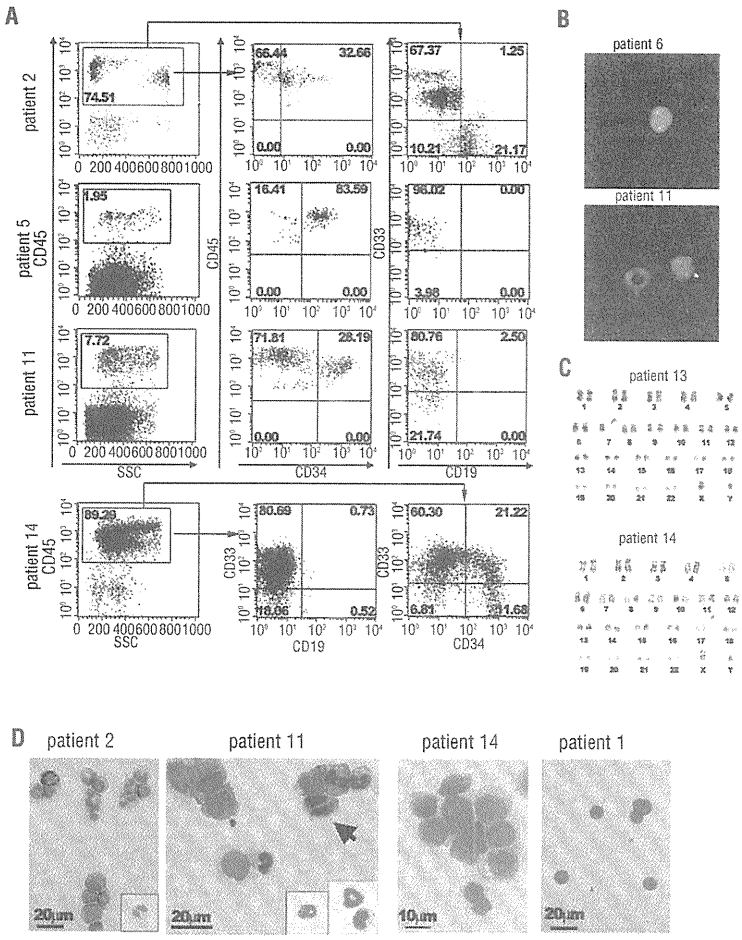

Figure 1. Engraftment of human MDS-originated hematopoietic cells in the bone marrow (BM) of NOG mice. (A) Representative flow cytometric profiles of BM cells recovered from mice engrafted with patients' BM cells. The majority of human CD45-expressing cells were positive for a myeloid marker CD33 in patients 5, 11, and 14, while some CD19$^+$ cells were present in BM cells recovered from the mouse engrafted with cells from patient 2. For patient 14, approximately one quarter of CD33$^+$ cells co-expressed CD34. The percentages of cells in the respective regions are shown. (B) FISH detection of a partial deletion of chromosome 7 and monosomy 7. Human cells recovered from the mice engrafted with BM cells from patient 6 and patient 11 were subjected to FISH analysis using D7Z1 (green signal for centromere of chromosome 7) plus D7S486 (red signal for 7q31 region) probes for patient 6 and D7Z1 (yellow signal) probe for patient 11. In a lower panel, a murine granulocyte with a ring-shaped nucleus which did not hybridize with the human probe is located adjacent to the human cell hybridized with D7Z1. All cells analyzed (10 cells for patient 6 and 100 cells for patient 11) demonstrated the same outcome. (C) Chromosomal analysis of cells recovered from the mice transplanted with MDS-originated cells obtained from the BM of patient 13 and patient 14 demonstrated the maintenance of the original abnormal karyotype, namely isochromosome 17 and monosomy 7 (arrows), respectively. Eight cells were analyzed for patient 13 and 20 cells for patient 14. (D) Wright-Giemsa-stained cytospin preparations made of CD45-sorted human cells. In the cytospin samples for patient 2, various stages of myeloid lineage cells and an eosinophil are shown. An insert shows a myelocyte with pseudo-Pelger anomaly. For patient 11, an arrow indicates a bi-nucleated myelocyte. Inserts show differentiated neutrophils. The majority of cells found in a cytospin preparation of BM cells obtained from the mice engrafted with cells from patient 14 demonstrated fine chromatin formation and conspicuous nucleoli. Cytospin samples of a normal cell-engrafted mouse (patient 1) were composed of lymphocytes.

Histological analysis of the bone marrow compartment of mice engrafted with myelodysplastic syndrome-originated cells

Successful engraftment of MDS-originated cells from six patients prompted us to dissect out the phenotypes of MDS-originated cells in the murine bone marrow environment. Although MDS is normally a disease of normal- to hyper-cellularity, the total number of bone marrow cells recovered from injected tibiae of the mice engrafted with MDS-originated cells was significantly lower than that of the mice engrafted with normal cells (Table 1, MDS-originated cell engrafted tibiae: 2.48±1.81 10^6, n=11, normal cell engrafted tibiae: 5.59±3.14 10^6, n=13, P=0.004). We then analyzed histological sections of mice engrafted with bone marrow cells from patients 11, 13, and 14. Consistent with the above finding, the marrow of the animals engrafted with MDS-originated cells from patient 11 appeared distinctly hypocellular compared to the marrow of normal cell-engrafted animals (Figure 2A). Human cells expressing human CD45, CD15, CD31, CD61, or glycophorin A (GlyA) were scattered throughout the marrow compartment in the injected tibiae of mice engrafted with normal cells or cells from patient 11. Neither human hematopoietic cells nor mesenchymal cells were observed in the contralateral tibiae of the same mice (Figure 2B and *data not shown*), consistent with our previous findings that intramedullary injected cells, especially when a limited number of cells were used, had a tendency to stay in the injected tibia.[16,18]

The cytology and bone histology of the mice engrafted with cells from patients 13 and 14 revealed that most of the marrow compartment was filled with large human CD45$^+$ leukemic blasts with prominent nucleoli (Figures 1D and 2A, and *data not shown*), leaving little space for normal murine hematopoiesis. Consistently, the number of non-human cells in the tibiae of mice engrafted with MDS-originated cells was significantly lower than that of the mice engrafted with normal cells (MDS-originated cell-engrafted tibia: 1.98±1.8 10^6, n=11, normal cell-engrafted tibia: 4.59±2.7 10^6, n=13, P=0.006). Although all experimental animals were irradiated equally, to exclude a possibility of heterogeneous response to sublethal irradiation as a cause of this decreased bone marrow cellularity in tibiae engrafted with MDS-originated cells, the number of non-human cells was also compared with that in the contralateral tibia of the same mice. The number of non-human cells in the injected tibia was significantly lower in the mice engrafted with MDS-originated cells (injected tibia: 3.08±1.35 10^6, contralateral tibia: 5.12±0.84 10^6, n=4, P=0.02), while there was no difference in non-human cell cellularity in mice engrafted with normal cells (injected tibia: 5.4±0.8 10^6, contralateral tibia: 5.2±1.2 10^6, n=3, P=0.4). The cell surface phenotypes of cells from patients 13 and 14 in murine bone marrow were primarily CD34$^+$, CD31$^+$, or CD61$^+$. Unlike the mice engrafted with normal cells or bone marrow cells from patient 11, the cells derived from patients 13 and 14 in the bone marrow rarely expressed CD15 or GlyA, two lineage markers used in this histological study.

Interestingly, proliferating primitive CD34$^+$ cells were prominently clustered along the endosteum, contrasting with the bone marrow of animals transplanted with nor-

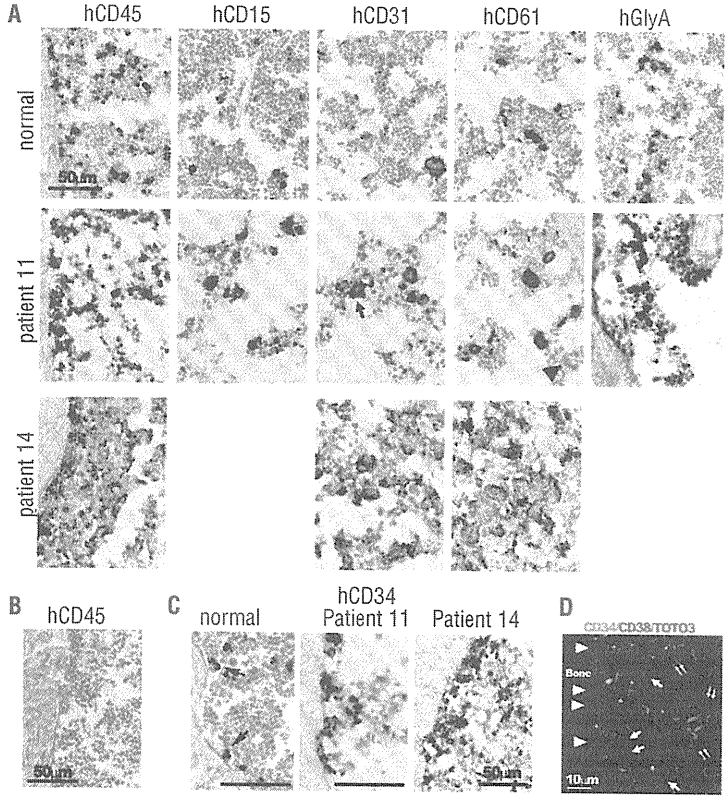

Figure 2. Histological analysis of human MDS-originated cells in murine bone marrow (BM). (A) Immunohistochemical staining of bone sections of the mice engrafted with BM cells from normal individuals and patients 11 and 14. Human cells were recognized by specific staining for human antigens. Cells that reacted with antibodies specific to human CD45, CD15, CD31, CD61, and glycophorin A (GlyA) were detected throughout the murine BM compartment in the bone samples of normal individuals and patient 11. Relatively small megakaryocytes with separated nuclei (an arrow) were often observed in the CD31 stained sections of the mice engrafted with cells from patient 11. Note, murine megakaryocytes are negative for human CD61 (an arrowhead), confirming the specificity of the antigen-antibody reaction. In bone samples of patient 14, human CD45-expressing cells occupied most of the marrow compartment. Cells expressing megakaryocytic markers, CD31 and CD61, were noticeable. (B) A human CD45-stained bone section of contra-lateral tibia of the mice intramedullary injected with MDS-originated bone marrow CD34$^+$ cells from patient 11 and MSC. Neither obvious hypocellularity nor human CD45$^+$ cells were detected. (C) In bone samples of patient 11, MDS-originated CD34$^+$ cells proliferated along the surface of the endosteum, while individual CD34$^+$ cells (arrows) attached to the endosteum in normal cell-engrafted mice. Invasion of CD34$^+$ cells was prominent in bones engrafted with cells from patient 14. (D) The cells expressing only CD34 (arrowheads) attached to the endosteum, but the cells expressing both CD34 and CD38 did not (arrows). The cells expressing only CD38 (double arrows) were located distant from the bone.

mal CD34⁺ cells in which individual CD34⁺ cells attached to the endosteum (patient 11, Figure 2C). The endosteal surface of primary recipient mice for patient 14 was covered with CD34⁺ cells, indicating an invasion of the putative hematopoietic stem cell niche by MDS-originated CD34⁺ cells (Figure 2C). Consistent with a previous report,[15] many of the MDS-originated CD34⁺ cells adhering to the endosteal surface lacked CD38 expression. The immunophenotypes of human cells gradually changed from CD34⁺CD38⁻ to CD34⁺CD38⁺, and eventually to CD34⁻CD38⁺ as cells were located further away from the endosteum (Figure 2D).

Sequential engraftment of myelodysplastic syndrome-originated cells

Serial transplants were conducted using bone marrow cells recovered from mice engrafted with bone marrow CD34⁺ cells from patients 11, 13, and 14. MDS-originated cells from patients 13 and 14, two patients whose cells demonstrated limited differentiation ability in murine bone marrow, but not from patient 11, successfully engrafted in secondary recipient mice (Figure 3A). In addition, it was possible to maintain the MDS-originated bone marrow cells from patient 14 for more than 2 years *in vivo* through passaging until the 8th recipient. The immunophenotypes of the engrafted cells were basically maintained throughout the experiments despite a gradual decline in the percentages of human cells over the period of the serial transplants. Interestingly, the frequency of CD34-expressing cells increased in the later transplant animals (*Online Supplementary Table S4* and Figure 3B), even though the frequency of CD34⁺ cells (%) in the endosteal area (within the distance of 5 cells) declined (53.79 ± 3.23, 40.56 ± 1.95, 38.85±0.87, and 29.88±6.74, for the 3rd, 5th, 6th, and 7th transplants, respectively), indicating a widespread distribution of primitive CD34⁺ cells and, thus, the selection or overgrowth of blastic cells against lineage differentiation. As expected, CD34⁺ cells, but not CD34⁻ cells, were able to sustain neoplastic cell growth into the next generation (*Online Supplementary Table S4*). Importantly, fluorescent activated cells sorting (FACS) analysis of human cells recovered from the engrafted mice demonstrated the maintenance of approximately the same proportion of CD34⁺CD38⁻ cells, a subpopulation of cells that includes leukemic stem cells,[13,15] until the 7th engraftment even though the overall human cell chimerism declined (Figure 3B).

Human cells were localized in the endosteal region in the

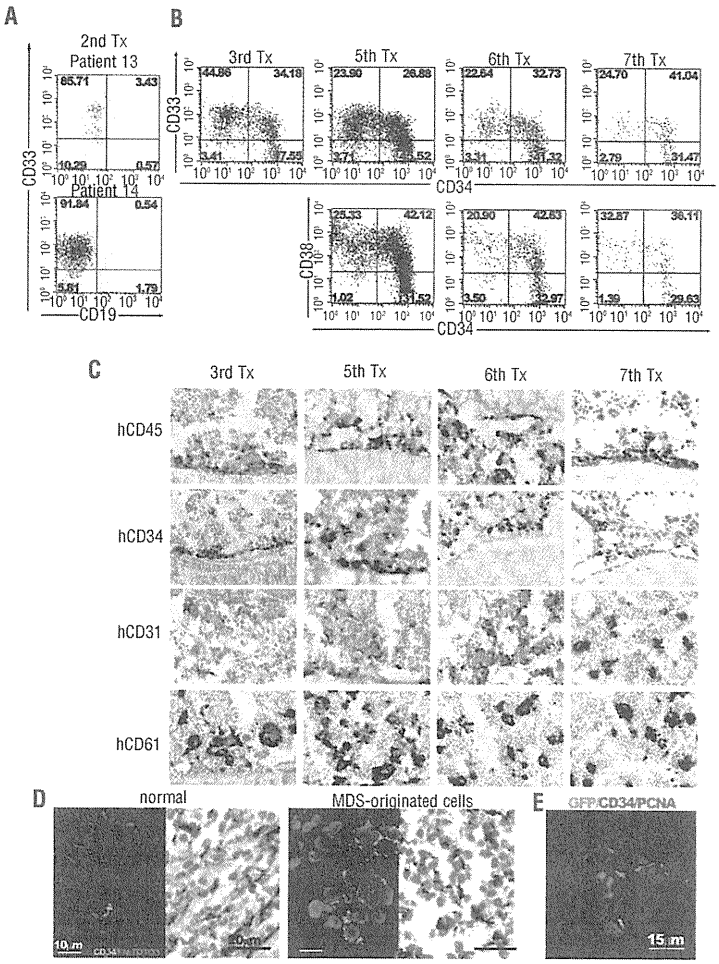

Figure 3. Serial transplantation of MDS-originated cells and the bone marrow microenvironment (A) Flow cytometric profiles of bone marrow (BM) cells recovered from secondary hosts. Tx indicates transplantation. (B) Flow cytometric profiles of BM cells recovered from mice that had undergone serial transplants with BM cells from patient 14. (C) Immunohistochemical staining of bones obtained from mice serially transplanted with cells of patient 14 demonstrated a lineage cell staining pattern similar to that of the primary recipient mice, while CD45 and CD34-expressing cells were more confined to the endosteal region. (D) Immunofluorescent and immunohisotochemical staining for fibronectin (FN) of bones of normal cell- and MDS-originated cell-engrafted mice. Murine and human cells in normal cell-transplanted mice were tightly enveloped by fibronectin while the fibronectin network of MDS-originated cell-engrafted mice was disrupted. A light field photograph confirmed the well-structured fibronectin network in the BM of normal cell-engrafted mice, but only fibronectin fibrils were detected in the MDS-originated cell-engrafted mice. Stained sections of the mice engrafted with cells from patient 11 are shown. The same staining patterns were confirmed in bone sections of mice engrafted with cells from patients 13 and 14. (E) MDS-originated CD34⁺ cells expressing a proliferating marker, PCNA, interacted with human MSC marked with green fluorescent protein.

bone marrow of serially transplanted mice, in contrast to the situation in the primary recipient mice in which human CD45$^+$ cells were ubiquitously located (Figures 2A and 3C). Even so, the MDS-originated CD34$^+$ cells occupied the murine endosteal surface, in striking resemblance to the situation in the bones of the primary recipients, thus indicating the persistence of leukemic stem cells, at least until the 6th transplant. Although the FACS analysis indicated the maintenance of a CD34$^+$CD38$^-$ subpopulation that included leukemic stem cells until the 7th serial transplant (Figure 3B), the 8th transplant did not result in obvious human cell engraftment (*Online Supplementary Table S4*). Consistent with this, in histological studies of the bone marrow of the recipient of the 7th transplantation, MDS-originated CD34$^+$ cells attached to the bone surface had disappeared (Figure 3C). These results are also consistent with our previous finding that CD34$^+$CD38$^-$ fractions are heterogeneous and stem cells reside at the endosteal surface.[22]

The microenvironment of mice engrafted with myelodysplastic syndrome-originated cells

The proliferation and survival of neoplastic cells are influenced by the host microenvironment. In this study, decreased bone marrow cellularity was a distinctive feature of all the MDS-originated cell engrafted samples analyzed (Table 1), thus indicating the suppression of murine hematopoiesis when neoplastic cells were present. To shed light on how neoplastic cells gained competitive advantages over normal host cells, the marrow compartments of animals engrafted with MDS-originated cells and normal bone marrow cells were examined. In the mice engrafted with normal bone marrow cells, the fibronectin network was well-structured throughout the marrow cavity (Figure 3D). In contrast, fibronectin network formation was irregular or disrupted in the mice engrafted with MDS-originated cells. Clusters of human CD34$^+$ cells were proliferating around the disrupted fibronectin fibrils in the central medulla of the bone marrow compartment. These observations, combined with an earlier histological finding that contralateral tibiae of the mice engrafted with MDS-originated cells exhibited normal cellularity (Figure 2B), suggest that the disruption of fibronectin network favors survival and proliferation of MDS-originated cells, while making it difficult to sustain normal hematopoiesis. In addition, CD34$^+$ cells with a proliferation marker, PCNA$^+$, were associated with co-transplanted MSC (Figure 3E) in MDS-originated cell engrafted bone marrow, which suggests the involvement of transplanted MSC in the engraftment, survival and proliferation of MDS-originated cells in the murine microenvironment.

Discussion

The recent development of mouse models of human acute leukemia are helping us to understand the phenotypes and physiology of leukemic stem cells. Although the engraftment of clonal MDS cells has been reported,[23,24] little is known about the behavior of MDS stem cells *in vivo* because of the difficulties of propagation of MDS cells up to a level that allows detailed investigation of MDS biology. In this study, in order to establish a reliable murine model for human MDS, bone marrow CD34$^+$ cells from patients with MDS and AML-MRC were co-injected with human MSC into the bone marrow of mice, a method proven to help engraftment and differentiation of human hematopoietic cells in the murine bone marrow microenvironment.[16,18,25] Successful engraftment of MDS-originated cells was observed in three out of six MDS cases (3 out of 8 mice engrafted with patients' cells) and three out of eight AML-MRC cases (9 out of 12 mice engrafted with patients' cells). Much to our surprise, the mice engrafted with MDS-originated cells uniformly exhibited significant decreases in the number of non-human bone marrow cells in the injected tibiae in comparison to the number of such cells in mice engrafted with normal cells, even when the percentage of human cells was less than 1% of total mononuclear cells. This is consistent with the fact that suppression of normal hematopoiesis can occur even when the tumor burden is relatively low. We found that most of the endosteal surface was covered with MDS-originated CD34$^+$ cells, a phenomenon also seen in murine models of acute leukemia,[14,15] which could be the underlying basis for the selective outgrowth of MDS-originated clones in patients over time.

The MDS-originated cells recovered from the human cell-engrafted mice maintained many characteristics of the original patients' cells, such as the cell surface phenotype and cytogenetic abnormalities. Unlike the previous two studies in which clonal abnormalities were detected in a fraction of cells,[23,24] we confirmed the presence of abnormalities in all cells examined by either FISH or chromosomal analysis, probably because purified bone marrow CD34$^+$ cells were used, rather than bone marrow mononuclear cells or T-cell-depleted blood or bone marrow cells. This makes our method more attractive for studying the behavior of MDS-originated cells *in vivo* because the majority, if not all, of the engrafted cells can be assumed to originate from clonal MDS cells. The majority of cells capable of engrafting in murine hosts were derived from patients carrying one or more genetic abnormalities (5/6; *Online Supplementary Table S1*). It is also noteworthy that four of those patients harbored an abnormality in chromosome 7, monosomy 7 or a partial deletion of chromosome 7, which is commonly found in Asian MDS cases and an indicator of aggressive disease with a poor prognosis.[26,27] On the other hand, five of eight cases that did not engraft or engrafted with normal cells were genetically normal. Taken together, the engraftment ability of MDS-originated cells positively correlated with the cytogenetic abnormalities of the patients.

In the current study, we attempted to explore the importance of MSC in engraftment of MDS-originated cells by comparison to non-bone marrow-derived stromal cells and the non-stromal component of bone marrow cells as auxiliary cells of transplantation. The presence of non-bone marrow-derived stromal cells (dermal fibroblasts) or non-stromal cells (cells of the CD34$^-$ fraction) did not help engraftment of MDS-originated cells. In contrast, the presence of MSC consistently improved engraftment of MDS-originated bone marrow CD34$^+$ cells. The pro-engraftment effect observed in our study could, therefore, be uniquely attributed to the presence of bone marrow-derived MSC. An investigation of how MSC help engraftment of human hematopoietic cells was beyond the scope of this study, but our observation of a physical interaction between MDS-originated CD34$^+$ cells and MSC (Figure 3E) suggests that MSC create a favorable environment for human MDS-originated cells to survive in the murine microenvironment, possibly through the physical interaction itself and

production of human cytokines, as indicated by our previous study.[18] It has been speculated that microenvironmental changes are involved in the pathogenesis of MDS.[28-30] However, since there was no significant difference in the engraftment of MDS-originated cells between normal (allogeneic-) and patient-derived (autologous-) MSC transplanted groups tested in this study, humanization of the microenvironment appeared more important, at least in our present study. One interesting finding in the serial transplantation study was that AML-MRC cells that had already engrafted in mice no longer required auxiliary cells or an intramedullary route of administration in subsequent transplants, perhaps because the cells with an ability to overcome hurdles to homing and engraftment in a murine host were selected during the serial transplants.

Local regulatory signals from the surrounding microenvironment to stem/progenitor cells play restrictive roles not only for normal cell development but also for tumorigenesis and metastasis.[31] It has also been reported that leukemic cells disrupt the behavior of normal hematopoietic progenitor cells by creating an abnormal microenvironment.[32] The microenvironment consists of heterogeneous types of cells and extracellular matrix proteins. Fibronectin is one of the major components of microenvironment structure. It was shown that mice lacking the enzyme needed to produce galactocerebrosides, a class of glycolipids in the nervous system, had an altered fibronectin network in the marrow microenvironment, which resulted in defective intramedullary lymphopoiesis and a hypocellular bone marrow.[33] Several studies found that interactions between leukemic cells and fibronectin prevented the apoptosis of leukemic cells from patients with AML, acute lymphocytic leukemia, and B-cell chronic lymphocytic leukemia, as well as leukemic cell lines *in vitro*.[34-37] In this study, mice engrafted with MDS-originated cells had an overall disruption of the fibronectin network in the bone marrow compartment and a striking decrease in the number of non-human bone marrow cells, indicating the importance of the three-dimensional structure of the fibronectin network in normal hematopoiesis. The reason for this fibronectin disruption and decrease in bone marrow cellularity are currently undetermined, but matrix metalloproteinases may play a role in creating a microenvironment that favors neoplastic cell growth over normal hematopoietic development. This idea is consistent with the results from previous studies demonstrating the increased matrix metalloproteinase production in cells obtained from MDS patients[38,39] and degradation of fibronectin by matrix metalloproteinases in a number of pathological processes.[40-43]

In summary, this study describes the establishment of a xenograft model of human MDS, using cells obtained from patients with low-risk MDS, high-risk MDS, and AML-MRC. Our murine xenograft MDS model consisted of human cell progeny, the majority of which, if not all, originated from clonal MDS cells and which demonstrated the defective cytological features of the original patients' cells. The efficiency of engraftment in the AML-MRC group was lower than that of *de novo* AML study.[15,44] This is probably because our AML-MRC group included patients with low percentages of blasts, formally categorized as having refractory anemia with excess blasts in transformation according to the French-American-British criteria. The study shows that the transplantability of neoplastic MDS-originated cells is partly determined by genetic abnormality and clinical aggressiveness of disease, which reflects the pathogenesis and progression of MDS towards leukemia.

Authorship and Disclosures

The information provided by the authors about contributions from persons listed as authors and in acknowledgments is available with the full text of this paper at www.haematologica.org.

Financial and other disclosures provided by the authors using the ICMJE (www.icmje.org) Uniform Format for Disclosure of Competing Interests are also available at www.haematologica.org.

References

1. Steensma DP, Tefferi A. The myelodysplastic syndrome(s): a perspective and review highlighting current controversies. Leuk Res. 2003;27(2):95-120.
2. Nimer SD. Myelodysplastic syndromes. Blood. 2008;111 (10):4841-51.
3. Heaney ML, Golde DW. Myelodysplasia. N Engl J Med. 1999;340(21):1649-60.
4. Haase D, Fonatsch C, Freund M, Wormann B, Bodenstein H, Bartels H, et al. Cytogenetic findings in 179 patients with myelodysplastic syndromes. Ann Hematol. 1995;70(4):171-87.
5. Parlier V, van Melle G, Beris P, Schmidt PM, Tobler A, Haller E, et al. Hematologic, clinical, and cytogenetic analysis in 109 patients with primary myelodysplastic syndrome. Prognostic significance of morphology and chromosome findings. Cancer Genet Cytogenet. 1994;78(2):219-31.
6. Raskind WH, Tirumali N, Jacobson R, Singer J, Fialkow PJ. Evidence for a multistep pathogenesis of a myelodysplastic syndrome. Blood. 1984;63(6):1318-23.
7. Tsukamoto N, Morita K, Maehara T, Okamoto K, Karasawa M, Omine M, et al. Clonality in myelodysplastic syndromes: demonstration of pluripotent stem cell origin using X-linked restriction fragment length polymorphisms. Br J Haematol. 1993;83(4):589-94.
8. Nilsson L, Astrand-Grundstrom I, Arvidsson I, Jacobsson B, Hellstrom-Lindberg E, Hast R, et al. Isolation and characterization of hematopoietic progenitor/stem cells in 5q-deleted myelodysplastic syndromes: evidence for involvement at the hematopoietic stem cell level. Blood. 2000;96(6):2012-21.
9. Van Etten RA, Shannon KM. Focus on myeloproliferative diseases and myelodysplastic syndromes. Cancer Cell. 2004;6 (6):547-52.
10. Uckun FM. Severe combined immunodeficient mouse models of human leukemia. Blood. 1996;88(4):1135-46.
11. Reya T, Morrison SJ, Clarke MF, Weissman IL. Stem cells, cancer, and cancer stem cells. Nature. 2001;414(6859):105-11.
12. Lapidot T. A cell initiating human acute myeloid leukaemia after transplantation into SCID mice. Nature. 1994;367(6464): 645-8.
13. Bonnet D, Dick JE. Human acute myeloid leukemia is organized as a hierarchy that originates from a primitive hematopoietic cell. Nat Med. 1997;3(7):730-7.
14. Ninomiya M, Abe A, Katsumi A, Xu J, Ito M, Arai F, Suda T, et al. Homing, proliferation and survival sites of human leukemia cells in vivo in immunodeficient mice. Leukemia. 2007;21(1):136-42.
15. Ishikawa F, Yoshida S, Saito Y, Hijikata A, Kitamura H, Tanaka S, et al. Chemotherapy-resistant human AML stem cells home to and engraft within the bone-marrow endosteal region. Nat Biotechnol. 2007;25(11):1315-21.
16. Yahata T, Ando K, Sato T, Miyatake H, Nakamura Y, Muguruma Y, et al. A highly sensitive strategy for SCID-repopulating cell assay by direct injection of primitive human hematopoietic cells into NOD/SCID mice bone marrow. Blood. 2003;101(8):2905-13.
17. Muguruma Y, Reyes M, Nakamura Y, Sato T, Matsuzawa H, Miyatake H, et al. In vivo and in vitro differentiation of myocytes